BRNO UNIVERSITY OF TECHNOLOGY

VYSOKÉ UČENÍ TECHNICKÉ V BRNĚ

FACULTY OF MECHANICAL ENGINEERING

FAKULTA STROJNÍHO INŽENÝRSTVÍ

INSTITUTE OF MATERIALS SCIENCE AND ENGINEERING

ÚSTAV MATERIÁLOVÝCH VĚD A INŽENÝRSTVÍ

TERNARY SHAPE MEMORY ALLOYS FABRICATION BY COMPACTATION OF MECHANICALLY ALLOYED POWDER FEEDSTOCKS

PŘÍPRAVA TERNÁRNÍCH SLITIN S TVAROVOU PAMĚTÍ KOMPAKTAČNÍMI PROCESY MECHANICKY LEGOVANÝCH PRÁŠKOVÝCH PREKURZORŮ

BACHELOR'S THESIS

BAKALÁŘSKÁ PRÁCE

AUTHOR   Samuel Seidl
AUTOR PRÁCE

SUPERVISOR   Ing. Jan Čížek, Ph.D.
VEDOUCÍ PRÁCE

BRNO 2016

Zadání bakalářské práce

Ústav:	Ústav materiálových věd a inženýrství
Student:	**Samuel Seidl**
Studijní program:	Strojírenství
Studijní obor:	Základy strojního inženýrství
Vedoucí práce:	**Ing. Jan Čížek, Ph.D.**
Akademický rok:	2015/16

Ředitel ústavu Vám v souladu se zákonem č.111/1998 o vysokých školách a se Studijním a zkušebním řádem VUT v Brně určuje následující téma bakalářské práce:

Příprava ternárních slitin s tvarovou pamětí kompaktačními procesy mechanicky legovaných práškových prekurzorů

Stručná charakteristika problematiky úkolu:

Mechanické legování vysokoenergetickými mlýnky je jedním ze základních postupů přípravy materiálů práškové metalurgie. Optimální volba parametrů zpracování může vést k přípravě mechanicky legovaných směsí, které mohou sloužit jako výchozí materiál pro další zpracování.

Díky svým specifickým vlastnostem získávají slitiny s tvarovou pamětí (SMA) v posledních letech zvýšenou pozornost. Nově bylo ukázáno, že kromě postupů odléváním lze tyto slitiny vyrábět též postupy práškové metalurgie.

Cílem práce bude pokus tvorby ternárních SMA slitin pomocí vhodně zvolených procesů kompaktace mechanicky legovaných práškových prekurzorů a následného tepelného zpracování.

Cíle bakalářské práce:

- seznámit studenta s problematikou slitin s tvarovou pamětí
- seznámit se s procesy mechanického legování práškových směsí a faktory ovlivňujícími vlastnosti připravených materiálů
- pokusit se zpracovat získaný prekurzor ternární slitiny zvoleným procesem kompaktace a následně jej tepelně zpracovat
- vyhodnotit strukturu a vlastnosti získaného materiálu

Seznam literatury:

Mohd Jani, J., Leary, M., Subic, A., Gibson, M. (2014): A review of shape memory alloy research, applications and opportunities. Materials Design, vol. 56, pp. 1078–1113, DOI: 10.1016/j.matdes.2013.11.084.

Tang, S. M., Chung, C. Y., Liu, W. G. (1997): Preparation of Cu-Al-Ni-based shape memory alloys by mechanical alloying and powder metallurgy method. Journal of Materials Processing Technology, vol. 63, pp. 307-312, DOI: 10.1016/S0924-0136(96)02641-6.

Pourkhorshidi, S., Naeimi, M., Parvin, N., Zamani, S. M. M., Ebrahimnia, H. (2012): Manufacturing and Evaluating of Cu-based Shape Memory Alloys by Hot Extrusion of PM Samples Made by Mechanical Alloying Process. Proceedings of Metal 2012 conference, Brno, Czech Republic.

Suryanarayana, C. (2001): Mechanical alloying and milling. Progress in Materials Science, vol. 46, pp. 1-184, DOI: 10.1016/S0079-6425(99)00010-9.

Termín odevzdání bakalářské práce je stanoven časovým plánem akademického roku 2015/16

V Brně, dne

L. S.

....

prof. Ing. Ivo Dlouhý, CSc.   doc. Ing. Jaroslav Katolický, Ph.D.

ředitel ústavu   děkan fakulty

ABSTRACT

The subject of Cu-Al-Ni shape memory alloy function and application is presented in this work. Further it discusses various approaches of producing such alloys, namely use of powder metallurgy procedures and compaction processes such as spark plasma sintering and heat treatment of prepared green compacts. These methods were also investigated in form of experiment and obtained results evaluated.

KEY WORDS

Shape memory alloy, Cu-Al-Ni Shape memory alloy, Spark plasma sintering, Powder metallurgy, Mechanical alloying

ABSTRAKT

Predmetom tejto práce je funkcia a použitie zliatiny s tvarovou pamäťou na báze Cu-Al-Ni. Ďalej sú skúmané rôzne prístupy vo výrobe týchto zliatín, konkrétne prášková metalurgia a kompaktačné procesy ako spekanie výbojom plazmy a tepelné spracovanie pripravených surových výliskov. Tieto metódy boli taktiež skúmané formou experimentu a výsledky vyhodnotené.

KĽÚČOVÉ SLOVÁ

Zliatina s tvarovou pamäťou, Zliatina s tvarovou pamäťou na báze Cu-Al-Ni, Spekanie výbojom plazmy, Prášková metalurgia, Mechanické legovanie

I declare that I have elaborated this bachelor's thesis on the theme " *Ternary shape memory alloys fabrication by compactation of mechanically alloyed powder feedstocks* " on my own, according to the instructions of my bachelor's thesis supervisor and with the use of the sources listed in Bibliography

Samuel Seidl

TABLE OF CONTENTS

1 INTRODUCTION

Humankind has always been on search of more effective solutions in every possible thing. This approach is evident also in production of materials. Shape memory alloys have been studied and investigated for about 80 years now, but some of their attributes still do not allow broader application of their interesting properties. Therefore scientists from all over the world are looking for ways how to make their production easier and more accessible. Powder metallurgy combined with mechanical alloying has exhibited good results in improvement of their attributes and generally presents interesting possibilities in cost reduction and time saving. The goal of this work is to examine different aspects of powder metallurgy procedures in order to provide a more effective solution for production of such alloys.

2 THEORETICAL PART

2.1 Shape memory alloys

2.1.1 Overview

As the technology improves and as the traditional materials are not able to offer necessary and desired properties, new types of materials are being designed and developed to satisfy these needs. A relatively new group of materials that can exhibit interesting properties is called Smart materials and such can be found among metals, ceramics and polymers. Their name implies that they are able to sense changes in their environment, such as temperature, stress, light, humidity, and electric and magnetic fields, and eventually respond to them in predetermined manners by changing their properties. This applies to mechanical and electrical properties, appearance, structure or function. [1] [2]

Shape memory alloys (SMAs) are metallic alloys which, after being deformed, can return to their original shape and size when subjected to adequate conditions such as temperature or in special case magnetic field. SMAs are polymorphic, they exist in two different phases and three different crystal structures – austenite, twinned martensite and detwinned martensite. Their names relate to the phases in iron-carbon system, where the austenite is also stable at higher temperatures and martensite at lower temperatures. Also the phase transformation between these two phases is very similar to the martensitic transformation defined in iron-carbon system. It is initiated by temperature change, it is diffusionless, involves an orderly shift of large groups of atoms and occurs very rapidly, and the degree of transformation is dependent on temperature. [1]

The Shape memory effect (SME) is dependent on this phase transformation. As the Fig. 2.1 shows, the alloy in its original form is in austenite phase. Upon cooling the alloy gets to a temperature when the austenite starts to transform spontaneously into a martensite phase. This temperature is described as martensite-start (M_s), and accordingly, the temperature at which is this transformation completed is described as martensite-finish (M_f). At this point the martensite is heavily twined, but after applying of stress, which is for example done in order to gain the desired shape, these twin-boundaries start to migrate and thus the crystal structure changes to a detwinned martensite. When the applied stress is removed, the desired deformed shape is retained as is it indicated in the Figure 2.1, but only upon condition of being under the M_f temperature. If the alloy is heated, it starts to undergo a reverse phase transformation as soon as the temperature reaches austenite-start (A_s) temperature and by the time it gets to a austenite-finish (A_f) temperature, meaning that all the martensite transformed to austenite, the alloy is fully recovered in its original shape and size. Therefore SME is a diffusionless. [1] [3]

It is important to notice, that M_f and A_s, and similarly M_s and A_f are not identical. The measure of this transition temperature difference is called hysteresis and it is illustrated in Figure 2.2. Hysteresis is one of the most important properties of SMAs and defines the potential of SMA application. Materials exhibiting small hysteresis results in fast SME reaction at certain temperature which is required for actuation applications. On the other hand, large hysteresis secures the retention of the predefined shape over a large range of temperatures. This property can be affected by the composition of SMA.

Based on the graphic interpretation of Figure 2.1, the above mentioned explanation of SME can be described as a One-way SME. From the same picture it is also obvious that there are two other SME mechanisms. The Two-way SME can be then described as a reversible transformation, when the material can remember it´s shape at low and at high temperature. The phase transformation therefore proceeds upon temperature change without the need of applying stress. But the alloy in order to exhibit such effect has to be specially tehrmomechanically treated, which is more commonly expressed as "SMA training". This includes for example shape memory training, pseudoelastic training, and thermal cycling training under a constant stress. [4] It is then obvious that preparation of such alloy is not as easy compared to those with One-way SME, but the benefits they bring will be presented in Application section. The last illustrated SME is called Pseudoelasticity or Transformational Superelasticity. This effect can only be exhibited between temperatures A_f and M_d, because the phase transformation is unlike the tow other precesse only stress-induced and above M_d temperature the alloy is deformed like an ordinary material. [5]
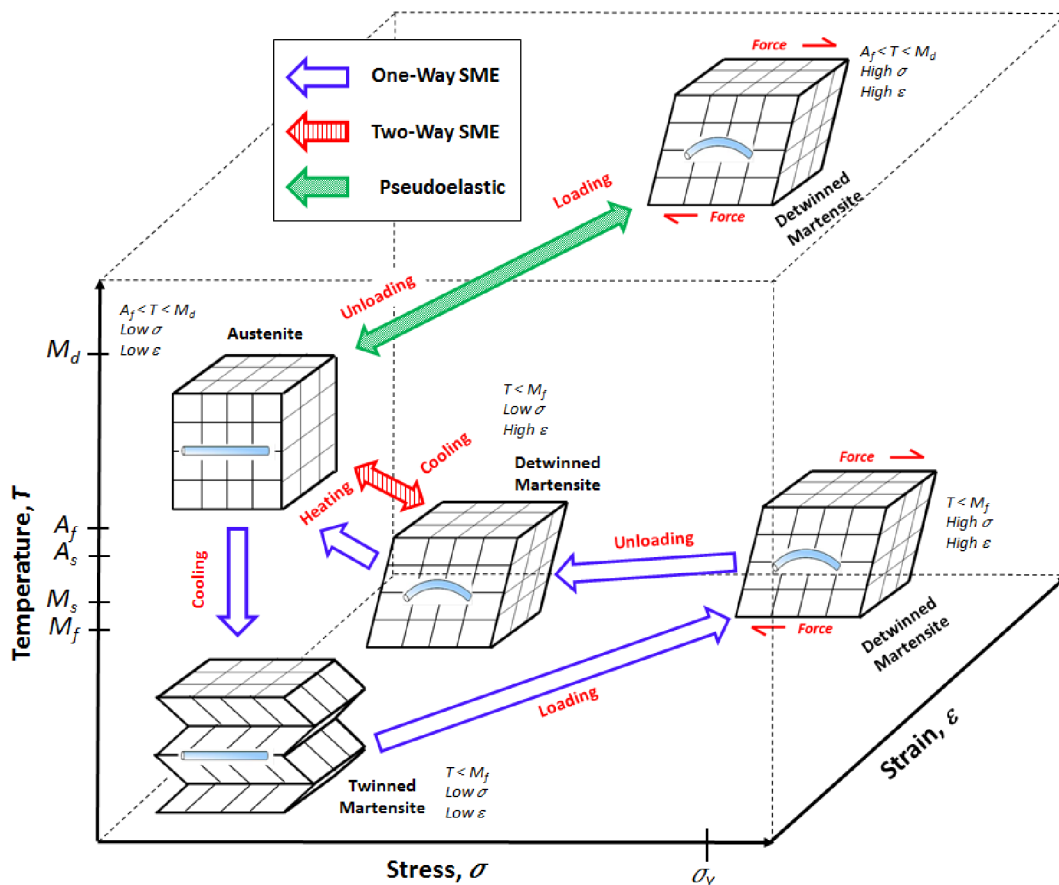

Fig. 2.1. Phase transformation of SMA [1]

However, SME has its limits, meaning, best SMAs nowadays can exhibit a maximum strain of 10%. If they are deformed more than that, they no longer fully exhibit SME. Most of the SMAs have a possible strain limit at approximately 3-5%. [1] This also has an effect on possible application of these alloys.

2.1.2 SMA Applications

Even though the first solid phase transformation in SMA was already observed in 1932, the first commercially successful application of the SMA was available in 1969, some years after the SME was observed in Ni-Ti alloy. [6] Since then the Ni-Ti alloy became the point of interest in various possible applications due to its reliability and better mechanical properties compared to the SMAs available at that time. Even nowadays, Ni-Ti based SMAs remain as the most convenient choice for SMA application.
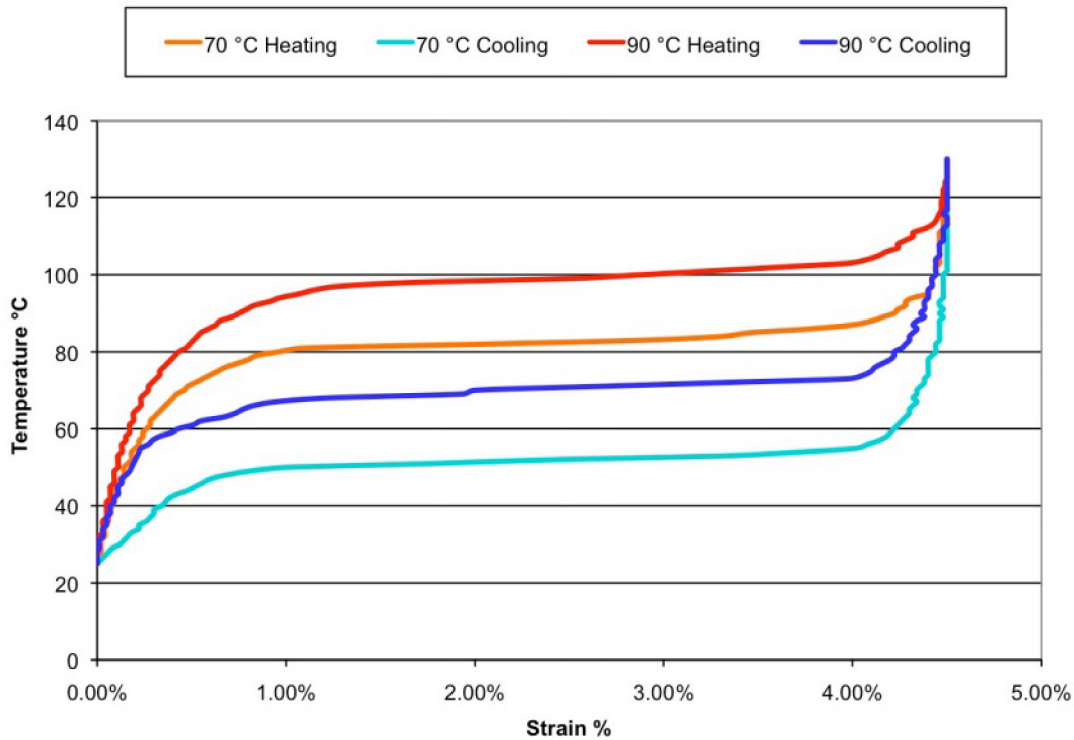
Fig. 2.2 Temperature vs. Strain Characteristics for Dynalloy's "LT" (70°C) and "HT"(90°C) NiTi alloy revealing the effect of hysteresis [7]

The ability of SMA to respond to changes in their environment or to react to outer stimuli directly provides a technical opportunity to replace conventional actuators like electric motors, pneumatics or hydraulics. Actuator, as defined by Merriam-Webster dictionary is „a mechanical device for moving or controlling something". But this is only one of the possible fields of application, therefore SMAs applications are herein summarized based on the SME abilities (Table 1) and according to the actual fields of use, some accompanied with a brief description of working principle.

2.1.2.1 Aerospace applications

The above mentioned first commercial success for SMAs was accomplished by Raychem Corporation with a CryoFit™ pipe coupler for hydraulic lines in F-14 fighter jet in 1969. This and other similar products for pipe coupling have a common working principle applying One-way SME. Such coupling is first machined out of Ni-Ti SMA at the room temperature. At this time the inner diameter is slightly smaller than the outer diameter of hydraulic lines which will be connected by it. Following this, coupling is cooled below the transformation temperature. While

being it martensitic state, the inner diameter of the coupling is expanded by a punch so that it would be bigger than the outer diameter of hydraulic lines for possible application, but the possible strain recovery has to be respected. The coupling has to be preserved at this temperature until it is installed. When coupling is brought back to the room temperature, it recovers its original shape and shrinks on to the hydraulic line, creating a metal to metal seal. The installation of such couplings is very quick and easy and does not require any expensive tooling. Over the years they have proven to be very reliable, exhibiting no leaks at all. [8]

A variable geometry chevron (VGC) for jet engine developed by Boeing is another successful application of SMAs. It was designed with the intent of optimizing engine performance. In this case, SMA flexure actuators are installed at the jet engine nozzle together with heaters. As SMA reacts to the temperature changes, it either maximazes the chevron deflection into the flow, which causes reduction of noise during take-off, or minimizes the chevron deflection, leading to an increased cruise efficiency during the remainder of the flight. [9]

There are many other interesting and progressive aerospace applications, to name few: wing morphing technologies, release or deploy mechanisms, vibration absorbing, rotor technology etc. [1]
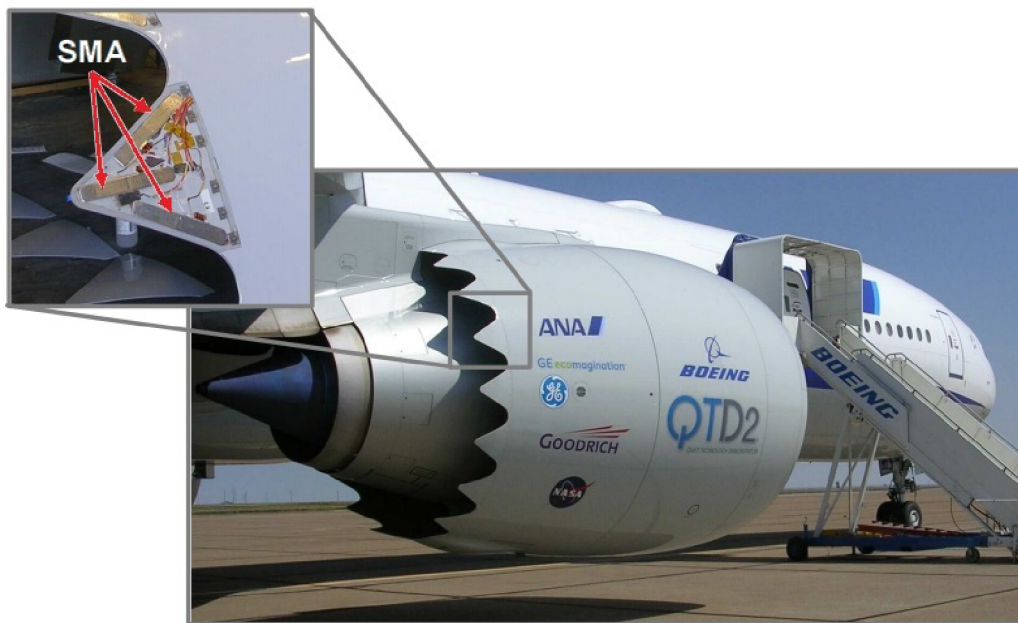

Fig. 2.3 Boeing VGC with detail of SMA flexure actuators position [10]

2.1.2.2 Automotive applications

In 1989 Mercedes-Benz introduced an automatic transmission with a thermally responsive pressure control valve, where the actuation task was executed by a thermal SMA Ni-Ti spring (Figure 2.4). In order to improve shifting comfort, the steel spring keeps the valve closed, thus reducing the shifting pressure until the transmission fluid reaches its operating temperature, which causes the Ni-Ti spring to recover to its original form and to generate force sufficient to open the valve. [11]

General Motors developed a SMA actuator to open and close hatch vent. This is located in the trunk of present generation Chevrolet Corvette. The actuator opens the hatch vent every time the deck lid is open enabling the air to be released easily form the trunk upon closing the lid. Once the trunk is closed, the actuator closes the vent

in order to maintain cabin temperature. The actuation task is performed by heating a SMA wire by passing of an electric current and subsequent cooling. [12]

Some other actuation applications include rear-view mirror folding, climate control flaps adjustment, engine temperature control, and lock/latch controls. SMA actuators and components have the potential to reduce the scale, weight and cost of current automotive components.
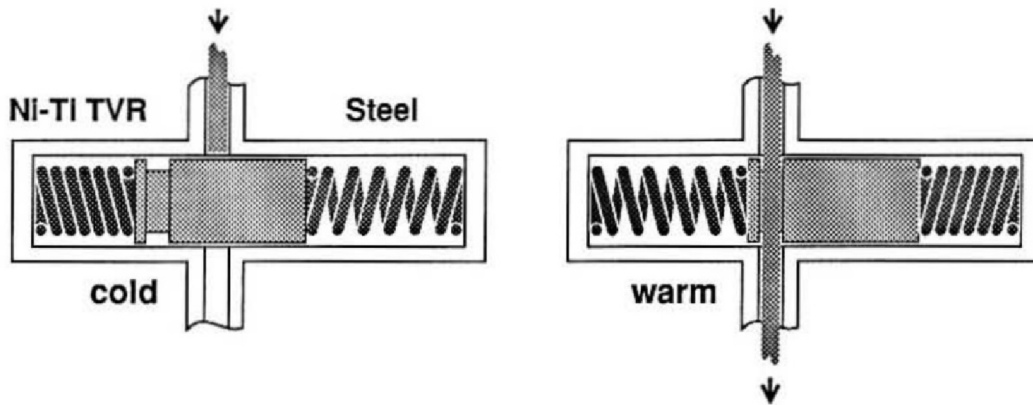

Fig. 2.4 Mercedes-Benz automatic transmission pressure control valve [11]

2.1.2.3 Biomedical and other applications

First biomedical application of SMA was introduced in 1971 by Andreasen, presenting superelastic braces made from Ni-Ti alloy. Over the years Ni-Ti alloys exhibited very good behavior for biomedical applications, especially due to their high corrosion resistance, bio-compatibleness, non-magnetic behavior and ability to respond and change accordingly to the temperature change of human body. Applications include stents, medical tweezers, anchors for attaching tendon to bone, guide wires, eyeglass frames and many more. [1]

SMAs are being also successfully used in robotic applications as micro-actuators or artificial muscles. SMA applications are being further investigated and improved. Some of the current development trends include morphing capability for aerodynamics and aesthetic features, high temperature actuators, noise, vibration and harshness dampers, efficient, stable and accurate actuators, etc.
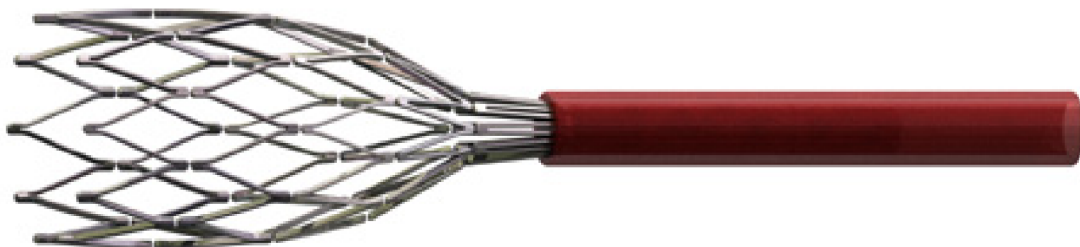

Fig. 2.5 NiTi stent self expands after being removed from endoscopic installation tube [13]

Table 1 Shape memory application categories [1]

Category	Description	Examples
FREE RECOVERY	The sole function of the memory element is to cause motion or strain on the applications **Working principle:** The memory element is stretched and then released (no load applied). It remains in stretched condition until heated above the transition temperature and shrink back to its original form, and subsequent cooling below the transition temperature does not cause any macroscopic shape change (e.g. OWSMA)	NiTi eyeglass frames (TiFlex™, TITANFlex®) and Simon IVC filter
CONSTRAINED RECOVERY	The memory element is prevented from changing shape and thereby generates a stress or force on the applications **Working principle:** The memory element is prevented from returning to its original form after being stretched and considerable force generated if heated above the transition temperature	Hydraulic couplings, fasteners and connectors: CryoFit™, Cryocon®, UniLok®, CryOlive®, CryoFlare®, CryoTact®, Permacouple®, Tinel Lock® and BetaFlex™
ACTUATOR OR WORK PRODUCTION (Force actuator, proportional control and two-way-effect with external reset force)	There is motion against a stress and thus work is being done by the memory element on the applications Most of applications fall in this category. Can be either OWSMA or TWSMA. Three types of actuators: **Force actuator:** The memory element exerts force over a considerable range of motion, and often for many cycles **Proportional control:** The memory element used only part of its selected portion of shape recovery to accurately position the mechanism, because the transformation occurs over a range of temperatures rather than at a single temperature **Two-way-effect with external reset force:** The memory element generates motion to overcome the opposing force, and thus do work. The memory element contracts upon heating to lift a load, and the load will stretch the heating element and reset the mechanism upon cooling (e.g. TWSMA)	Electrical actuators (VEASE™, SMArt Clamp™), thermal actuators (Memrysafe®, circuit breaker, window or louvre opener, valves), and heat engines
SUPERELASTICTY	The applications are isothermal in nature and involve the storage of potential energy	Eyeglass frame, orthodontic archwire, Mammelok® breast hook, guidewires, anchors and underwire brassiere

2.1.3 Cu-Al-Ni based Shape memory alloys

Shape memory effect in Cu-Al-Ni based alloy was first observed in 1964. [14] This type of alloy typically contains 11-14,5% Al and 3-5% Ni. [15] Cu-Al-Ni system has number of characteristic phases which define final properties of these alloys as for example described in [16], and [17]. In recent years it has been given bigger attention and it has undergone extensive development, because this kind of SMA is made from relatively inexpensive elements, which makes it commercially available, it presents higher thermal stability than Cu-Zn-Al or Ni-Ti alloys whose maximum working temperature is around 100 °C, whereas the possible use of Cu-Al-Ni SMAs is at temperatures near 200°C, and it´s recovery force is second best after Ni-Ti SMA. On the other side, Cu-Al-Ni SMAs are brittle due to their very high elastic anisotropy and large grain size, and in general show poor mechanical properties, which severely limit their industrial applications. Large grain size is an effect of preparing this alloy by conventional casting methods, because those exhibit difficulties in controlling the grain size. However, there have been made many efforts with objective of improving this type of alloy, for example by refining the grain size by adding other elements to the traditional Cu-Al-Ni system, by using powder metallurgy and mechanical alloying [18] [19], or by fabricating a single crystal alloy. [17] French company Nimesis Technology is one of the successful producers of this type of alloy both with polycrystalline and monocrystalline structure.

2.2 Mechanical alloying

Alloying as a process has been known ever since humankind started using metals. First it may have been just an act of coincidence adding or mixing one kind of metal with other type of metal, but in course of time, people have learned of various advantages and disadvantages that these operations carry along with them. Knowledge about combining elements has been carried on, further examined, many experiments have taken place and many techniques have been developed which all lead to production of materials with desired properties.

The mechanical alloying (MA) process was developed as a result of searching for reasonable way of producing nickel-based superalloy for gas turbine application, which had to combine high-temperature strength of oxide dispersion and the intermediate-temperature strength of gamma-prime precipitate. This technique was developed and summarized by John Benjamin and his colleagues at the Paul D. Merica Research Laboratory of the International Nickel Company (INCO) in 1968. , and can be described as a powder processing technique that allows production of homogeneous materials starting from blended elemental powder mixtures. [20] [21]

"The actual process of MA starts with mixing of the powders in the right proportion and loading the powder mix into the mill along with the grinding medium (generally steel balls). This mix is then milled for the desired length of time until a steady state is reached when the composition of every powder particle is the same as the proportion of the elements in the starting powder mix. The milled powder is then consolidated into a bulk shape and heat treated or any other powder sintering method is used to obtain the desired microstructure and properties. Thus the important components of the MA process are the raw materials, the mill, and the process variables. Occasionally, metal powders are milled with a liquid medium and this is

referred to as wet grinding; if no liquid is involved then it is referred to as dry grinding." [21]

During MA, the whole load of mill is exhibited to number of forces created by the movement of mill (Figure 2.6). Powder particles then collide with grinding medium resulting in heavy deformation, as illustrated in Figure 2.7. This leads to creation of variety of crystal defects such as dislocations, vacancies, stacking faults, and increased number of grain boundaries. These defect structures enhance the diffusivity of solute elements into the matrix. Another effect of the deformation is a refinement of particles and also their microstructural features, which decrease the diffusion distances. Above mentioned collisions are also source of energy. This energy is transformed into a rise in temperature during milling, which also aids the diffusion behavior, and consequently, true alloying takes place amongst the constituent elements. Normally this process takes place at room temperature, but sometimes it may be necessary to anneal the mechanically alloyed powder at an elevated temperature for alloying to be achieved, apart from the temperature that is created by energy dissipation. This is particularly true when formation of intermetallics is desired. [21]
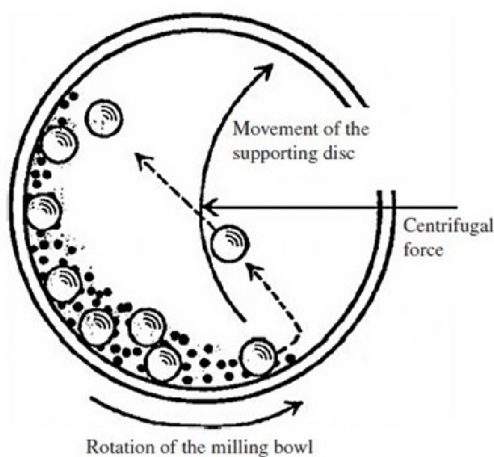
Fig. 2.6 Illustration of motion in planetary mill [22]
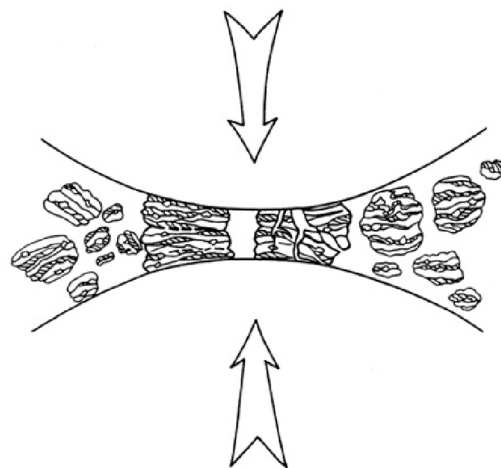
Fig. 2.7 Steel balls deforming powder particles [21]

Because mechanical alloying is a complex process, it involves optimization of a number of variables to achieve the desired product phase and/or microstructure. Some of the important parameters that have an effect on the final constitution of the powder are:

- type of mill (planetary ball mill, shaker mill, attritor mill, etc.)
- milling container (vial, bowl),
- milling speed,
- milling time,
- type, size, and size distribution of the grinding medium ,
- ball-to-powder weight ratio (BPR),
- extent of filling the vial,
- milling atmosphere,
- process control agent, and

－ temperature of milling.

All these process variables are not completely independent. For example, the optimum milling time depends on the type of mill, size of the grinding medium, temperature of milling, ball-to-powder ratio, etc. [21]

2.3 Compaction methods
Compaction of powders is a necessary step in powder metallurgy technique. Powder metallurgy like traditional casting methods enables production of final products with very little or no necessary finishing operations, but exhibits better ability in controlling final chemical composition and structure of final product. [23] Interparticle distances have to be reduced for bonding creation and final compact structure of product. There are various ways how this can be accomplished [24] [25], but this work due to its objective presents and describes only two of them.

2.3.1 Uniaxial pressing
Uniaxial pressing is one of the simplest methods of preparing a green compact for sintering. A hydraulic or mechanical press is normally used for this type of operation. [26] [24] The actual compaction process starts by filling a die with a powder of certain composition. Compaction or pressing within fixed dies can be divided into single action pressing and double action pressing. [24] Compaction procedure is illustrated in Figure 2.1. In stage 1 the powder is at its initial as filled state. After applying a pressure particles are forced to be re-arranged, to move to various positions where space is available and subsequently as the particles get closer to each other the density rises. This is illustrated as stage 2. When all the available space is used up and no further re-arrangement is possible, then first plastic deformations among the particles start to occur. By raising the pressure even more, the plastic deformation eventually results in creating cohesion between two surfaces which is also called cold welding. This gives the powder its structural integrity which allows it to be further processed as a green compact (stage 3).
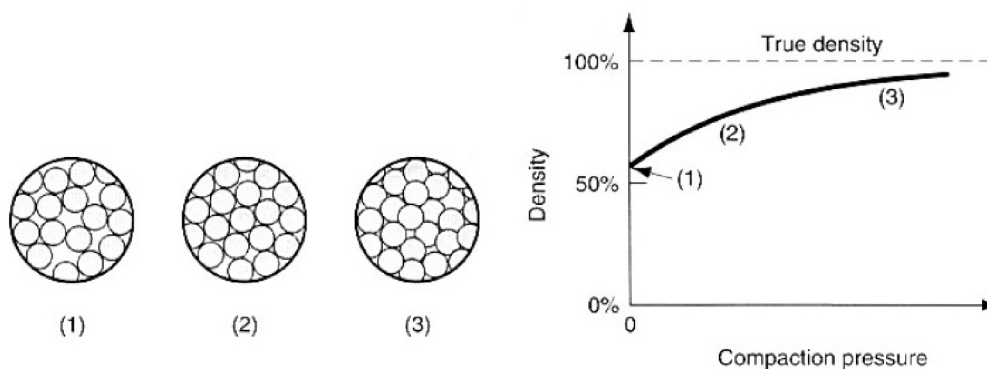
Fig. 2.8 Effect of compaction pressure on green compact density [27]

2.3.2 Spark plasma sintering
Spark plasma sintering (SPS) is a sintering technique combining uniaxial force and a pulsed (on-off) direct electrical current (DC) under low atmospheric pressure or protective gas to perform high speed consolidation of the powder. As the actual mechanism is partially unclear, even though the name indicates a creation of plasma

during this process, this technique is also described as pulsed electric current sintering (PECS). For the purpose of this work and further references, it will be referred to this technique as SPS. [28]

Figure 2.9 provides a detailed description of SPS device. The mechanical part resembles of uniaxial hydraulic press, but in this application hydraulic rams are water cooled and function as electrodes that transfer electric current to the die and powder. The die is normally made out of graphite due to its great conductivity and heat resistance and is placed between the upper and lower ram in a water cooled vacuum chamber. SPS devices offer broad variety of sintering options, because pressure, pulsed current, heating ratio and other things can be easily set up through control system. As already mentioned in the beginning of this section, there is no unanimous opinion on the actual sintering process mechanism, but for an illustration an explanation by Aalund is presented in this work. [29]
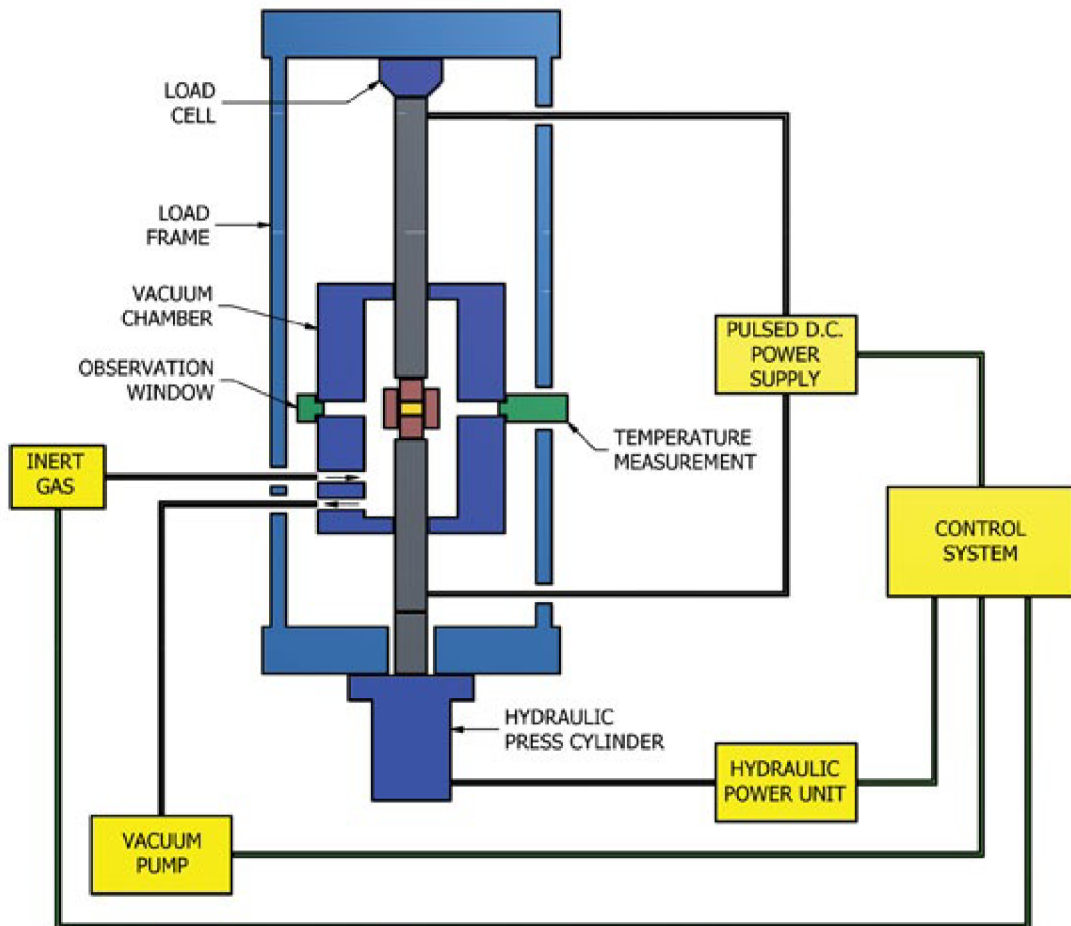
Fig. 2.9 Simple scheme of SPS machine [26] (Reprinted with permission of Ceramic Industry)

"SPS utilizes uniaxial force and ON-OFF DC pulse energizing. The ON-OFF DC pulse voltage and current creates spark discharge and Joule heat points between material particles (high-energy pulses at the point of intergranular bonding). The high frequency transfers and disperses the spark/Joule heat phenomena throughout the specimen, resulting in a rapid and thorough heat distribution, high homogeneity and consistent densities. The initiation of the spark discharge in the gap between particles is assisted by fine impurities and gases on and between the surfaces of the

particles. The spark discharge creates a momentary local high-temperature state of up to 10,000°C, causing vaporization of both the impurities and the surfaces of the particles in the area of the spark. Immediately behind the area of vaporization, the surfaces of the particles melt. Via electron draw during ON TIME and the vacuum of OFF TIME, these liquidized surfaces are drawn together, creating "necks." The ongoing "radiant" Joule heat and pressure causes these necks to gradually develop and increase. The radiant heat also causes plastic deformation on the surface of the particles, which is necessary for higher-density applications. During the SPS process, heat is concentrated primarily on the surfaces of the particles. Particle growth is limited due to the speed of the process and the fact that only the surface temperature of the particles rises rapidly. The entire process - from powder to finished bulk sample - is completed quickly, with high uniformity and without changing the particles' characteristics." [29]

SPS enables to sinter materials that are difficult to sinter by conventional methods, produces high density compacts with fine microstructure and exhibits short sintering times. Great results have been accomplished for sintering of cutting tool materials, biomaterials, materials for nuclear energy applications, nanomaterials and materials with low coefficient of thermal expansion (i.e. ceramics). [28]

3 EXPERIMENTAL PROCEDURES

3.1 Materials

Powder feedstocks for compaction were prepared by initial mixing of commercially available Cu, Al and Ni powders by GTV GmbH company. The blends were subsequently mechanically alloyed (MA) in Fritsch Pulverisette 6 planetary mill using two different milling times and speeds [30]. In both cases, 50 g of powder were placed in stainless steel vial together with hardened steel balls of 10 mm in diameter in 5:1 ball-to-powder ratio (BPR). Vial was filled with 100 ml of ethanol to cover both balls and powder and then, after sealing the vial, the remaining volume was pressurized with nitrogen gas to replace the remaining air, which could cause oxidation of powders. [30]

Table 2 Specifications of initial powder mixture

	Cu powder	Al powder	Ni powder
Product number	30.55.3	30.54.1	80.56.1
Purity (%)	99	99	99
Composition (wt%)	82	14	4

Table 3 Milling parameters and final composition

	Milling speed (rpm)	Milling time (hr)	Chemical Composition (wt%)			
			Cu	Al	Ni	O
Powder 1	400	10	39	30	2	29
Powder 2	300	50	46	33	3	18
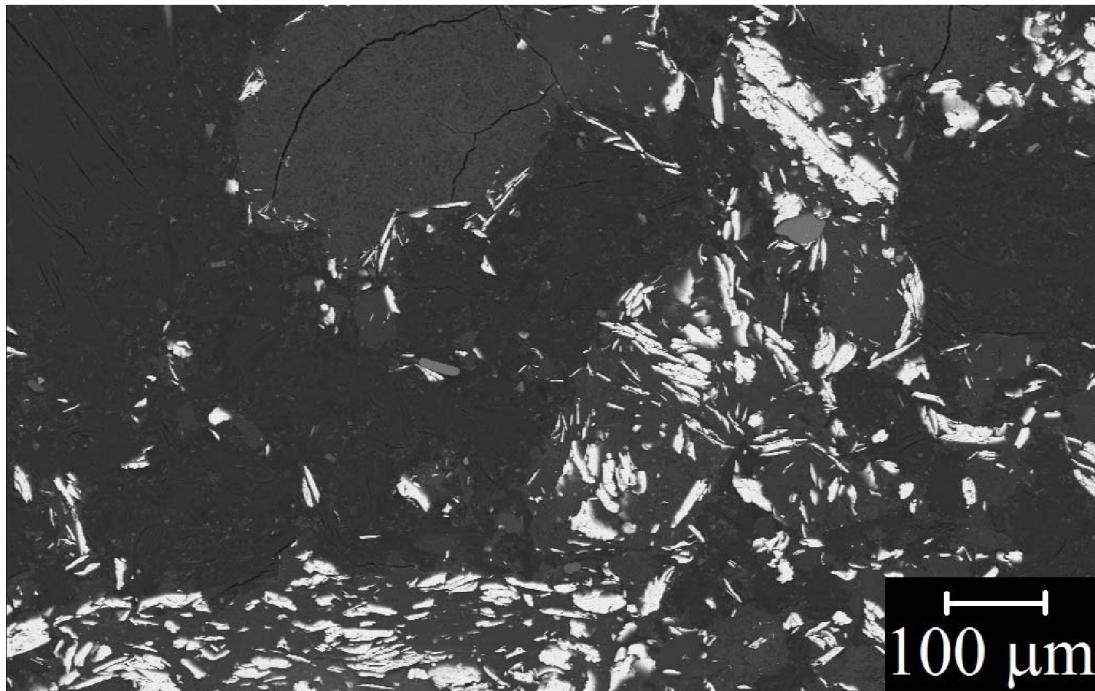
Fig. 3.1 Powder 1 internal structure (cross-section)
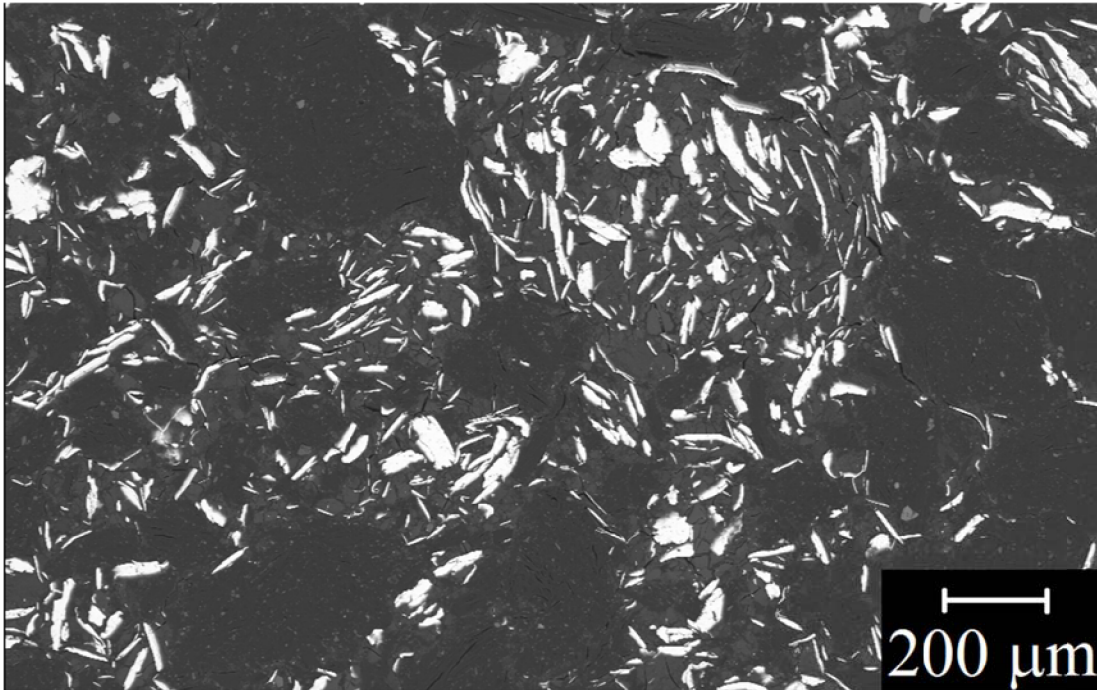
Fig. 3.2 Powder 2 internal structure (cross-section)

3.2 Compaction methods

3.2.1 Spark plasma sintering

Compaction process was performed on Thermal Technology LLC SPS Model 10 – 4. 3,5-4 grams of powder were used for every specimen in order to obtain compacts of similar thickness, the actual amount of powder did not have any noticeable effect on the internal structure of the compact . Powder was placed in a graphite die of 20 mm bore, using 2 layers of graphite paper to separate it from the walls of the actual die and also two layers of graphite paper on both top and bottom to separate it from graphite punches. The die was prepared for SPS on a small hydraulic press using pressure of 3 MPa to secure an even distribution of the powder inside of it. Following this the die was placed into the SPS chamber where it was preloaded by pressure of 5 MPa. Three different sintering parameter sets were used for both powders. For all samples, the pulse current was applied while the powders were loaded with the maximal predefined pressure. The non-continuous 120 ms pulses were separated by 30 ms idle pauses. All procedures were carefully monitored and recorded in graphic form, and the results and history thereof is attached in Appendix 1. The used sintering parameters are further provided in detail herein.

SPS1: Powder was loaded with 20 MPa and then heated to 600 °C by a heat rate of 100 °C/min. When the desired temperature was reached, the compact was loaded with 60 MPa for 8 minutes and then the pressure relieved to 20 MPa again. The compaction process was followed by a cooling phase at the rate set at 100 °C/min. In reality though the temperature decrease exhibited rather non-linear character, as could be seen from Appendix 1. When the system

temperature reached the room temperature, pressure was dropped to the initial 5 MPa.

SPS2: Powder was loaded with 20 MPa and then heated to 550 °C by a heat rate of 100 °C/min, followed by 40 minutes of dwell at this temperature. Subsequently the temperature was risen to 600 °C by the same heat rate as mentioned earlier and pressure of 60 MPa was again applied for 8 minutes. The cooling phase way identical as described in SPS1.

SPS3: Powder was loaded with 20 MPa and then like in SPS2 heated to 550 °C, but this time with a heat rate of 50 °C/min with a dwell of 40 minutes. Following that the temperature was raised to 920 °C by the heat rate of 50 °C/min and when the final temperature was reached a pressure of 60 MPa was applied. Cooling procedure was also in this case the same as described in SPS1.

3.2.2 Cold compaction and tube furnace sintering

Prepared powders were filled into 20 mm bore stainless steel die in between upper and lower punch and green compacts were prepared on a hydraulic press applying uniaxial pressure of 900 MPa. The green compacts were subsequently cut in half to secure a stable placement in a ceramic boat-shape vessel. The sintering procedure of green compacts was performed in a tube furnace Heraeus ROS 4/50 at 920 °C for 20 hours under a protective argon 4.6 (degree of purity) atmosphere of flow rate at 4 liters/minute, followed by quenching in room temperature water. Compacts prepared in this way are marked „CP".

3.3 Specimen preparation

SPS compacts were cut on Struers Discotom-2 Abrasive Cutter and hot mounted using Leco PR-4X Mounting Press. The tube furnace sintered compacts were cold mounted using Struers EpoFix epoxy resin combined with hardener according to the producer´s guidelines. All specimen were grinded for 2 minutes at each abrasive paper of grit size as follows (European marking): 500, 800, 1200, 2400, 4000. Polishing was executed by first using 3 μm polishing cloth combined with D 2 diamond paste for 2 minutes, then 1 μm polishing cloth combined with D 0,7 diamond paste also for 2 minutes, and finally 1 μm polishing cloth and adding Oxide Polishing Suspension for 2 minutes, which was replaced with water for another 2 minutes. Because specimen „SPS1-1" to „SPS3-2" were mounted in 50 mm discs, Leco GPX 300 Grinder/Polisher was used for both grinding and polishing operations, whereas specimen „CP1" and „CP2" due to their mounting disc size of 32 mm were grinded and polished by using Struers Dap-7 Grinding and Polishing Machine. The annotation of the specimens is provided in Table 3.3.

3.4 Analysis and characterization

3.4.1 Light microscopy

Optical analysis of sintered compacts was performed on Zeiss Axio Observer Z1 microscope. The objective of using this method was to observe, whether the sintering operations had the desired effect on the final structure, namely to see, if the diffusion process was fully completed, i.e. to find out, if there were still any distinguishable

traces of original elements, and if the structure had desired shape and size, optionally to examine porosity of the prepared compacts.

Table 4 Specimen identification

Specimen	Sintering method	Powder
SPS1-1	SPS1	1
SPS2-1	SPS2	1
SPS3-1	SPS3	1
SPS1-2	SPS1	2
SPS2-2	SPS2	2
SPS3-2	SPS3	2
CP1	CP	1
CP2	CP	2

3.4.2 Scanning electron microscopy

Scanning electron microscopy (SEM) Zeiss Ultra Plus device was used to obtain more detailed reference to the structure of compacts, to analyze grain growth, determine particle boundaries. Simultaneously energy-dispersive X-ray spectroscopy (EDX) analyses of all the compacts were performed to determine, how successful was the diffusion process by observing the chemical concentration and distribution of original elements.

3.4.3 X-ray Diffraction

Rigaku SmartLab 3 kW XRD scanner helped to examine phase composition of compacts, and to detect a prospective oxidation, formation of new phases such as intermetallics, solid solutions.

4 DISCUSSION OF RESULTS

4.1 Attributes of powder feedstocks

It is important to mention and discuss the composition of prepared powders at this place because it may have an effect on the composition of sintered compacts. Based on the data from Table 2 and Table 3, which were obtained by EDX analysis, it is clear that both powders after milling do not possess the same composition as the initial powder mixture. In both cases the proportion of Cu is less than a half compared to the initial powder, similarly the proportion of Ni is slightly smaller. Interestingly the proportion of Al is approximately two times bigger and presence of previously absent element O was detected. Mapping function revealed distribution of these elements in powder feedstocks.

When applied to Fig 3.1. and Fig 3.2, the bright particles represent Cu and dark particles are combination of Al and O. Both SEM and light microscopy confirmed Ni particles to be mostly contained in or close to Cu particles, which is the desired effect of mechanical alloying. The best results of alloying exhibited Powder 2 (Fig 4.1). However, some independent Ni particles were also found in both Powder 1 and Powder 2. Whereas bright Cu-Ni particles have mostly lamellar structure and similar sizes, Al-O particles are observed to have uncertain shape and various sizes and many of them are cracked. XRD analyses helped to investigate attributes of these powders from a view of phase composition. Both Powder 1 and Powder 2 did not exhibit any formation of Al phases, detected were only Cu and Ni.

All these facts lead to a conclusion that especially Al was very much affected by energy produced by collisions in milling vial due to high milling speed in the case of Powder 1 and long milling time in the case of Powder 2 and eventually transformed together with O to an amorphous phase [21], which cannot be detected by XRD analysis. Along with that it resulted in depleting of plasticity and subsequent initiation of cracks and breaking of particles. [30] A premise has been made that compacts made of Powder 2 should exhibit better composition of final structure especially due to its finer grain size and better state of alloying.
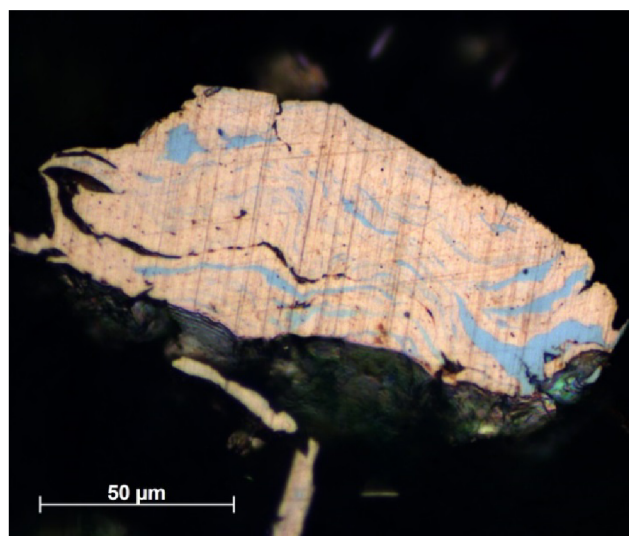
Fig. 4.1 Powder 2 particle showing Ni being part of Cu

4.2 Attributes of sintered compacts

4.2.1 Effects of compaction process

Additional attributes of behavior of the powder feedstock were observed during the compaction processes. Green compacts obtained by uniaxial pressing did not exhibit desired cohesion. This was observed especially while cutting the green compacts in preparation for heat treatment. While sowing, green compacts started to crumble and before being completely separated by sowing they broke. The green compacts were so brittle they could have been broken in hand, but it is important to notice, the approximate thickness of compacts was 4 mm. Even though the cohesion of powder feedstocks was not ideal for both powders, interestingly Powder 1 exhibited better cohesion over Powder 2 green compacts, as the previously mentioned breaking test had proven. This also had an effect on subsequent specimen preparation after the heat treatment and quenching was finished, as CP2 could not have been properly grinded nor polished, most likely due to its fine structure and poor cohesion among powder particles, which had not improved even by exhibiting the green compact to a high temperature for considerably long time. An oxide layer originated in exposing CP1 and CP2 to air and water and thus these specimens could have been further studied after first undergoing grinding and polishing processes.

However, a simultaneous combination of applied pressure and heat during SPS process resulted in production of dense solid compacts as Fig. 4.2 and Fig. 4.3 show. Temperature had an effect on final thickness of sintered compacts, as the ones sintered at 920 °C were the thinnest. Among all of them was almost no porosity found. Powder 2 exhibited rapid expansion during the first heating in all 3 SPS processes. Expansion represented by the violet line in Appendix 1 also occurred in case of Powder 1, but in this case it can be reasoned by a material dilatation as a result of rising the temperature since the changes in punch displacement were not so major. Therefore at this time there cannot be presented any valid reasons of behavior observed in processing of Powder 2.

Fig. 4.2 SPS1-1, SPS2-1 and SPS3-1

Fig. 4.3 SPS1-2, SPS2-2 and SPS3-2

4.2.2 Structural analysis

Structures of all 8 sintered specimens were analysed using both SEM and light microscopy. Unity of specimen orientation was kept in both CP and SPS specimen while taking pictures for better comparison. As the SPS specimen (Fig 4.4 - 4.9) sintering parameters varied mostly in sintering time and temperature (pressure was same for all), the effect of these two variables can be discussed. The effect of sintering time can be observed by comparing specimen SPS1-1 with SPS2-1 and SPS1-2 with SPS2-2. Images indicate that there are no major differences in the structure of these specimens. Therefore it seems reasonable to claim that temperature is among the important parameters to consider when sintering. There is a visible difference when comparing specimen SPS2-1 with SPS3-1 and SPS2-2 with SPS3-2. The structure of compacts processed by SPS3 is more ordered and even the dark Al-O particles with depleted plasticity seem to adjust to the effect of pressing and distribute themselves more evenly in the volume. Same effect can be observed in CP1. Due to the very brittle and crumbling structure of CP2, its structure cannot be adequately compared to the other specimen, even though Fig 4.5 at least partially shows better sintering among bright Cu particles.
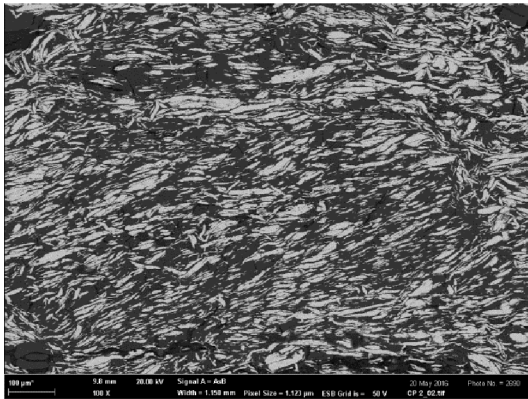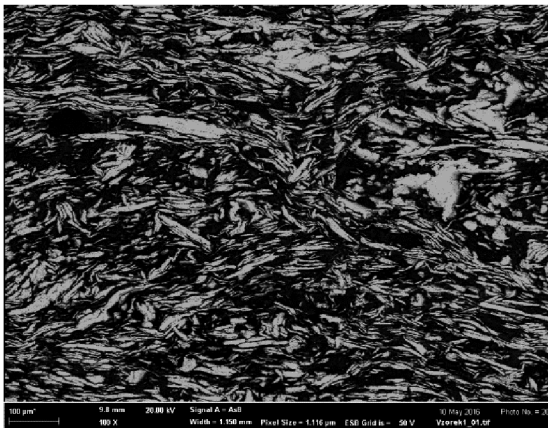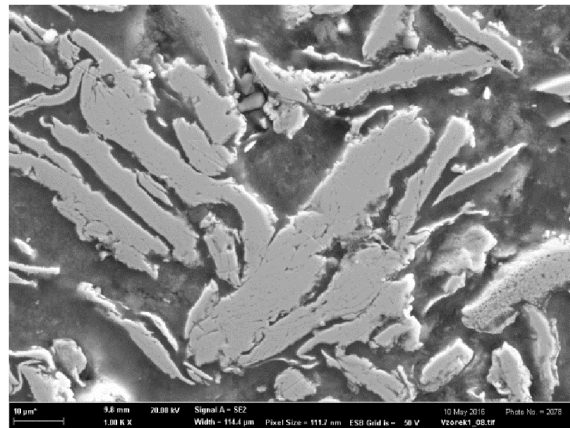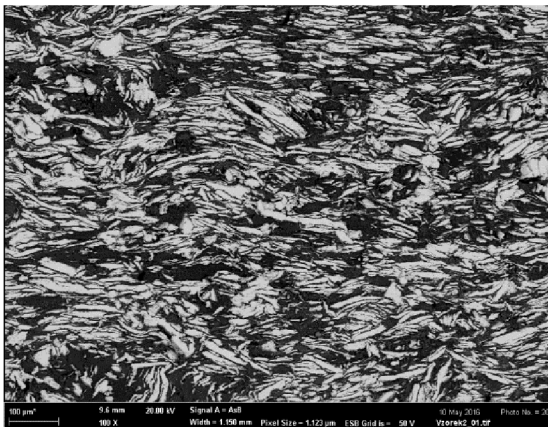

Fig. 4.2 CP1 magnification 100x
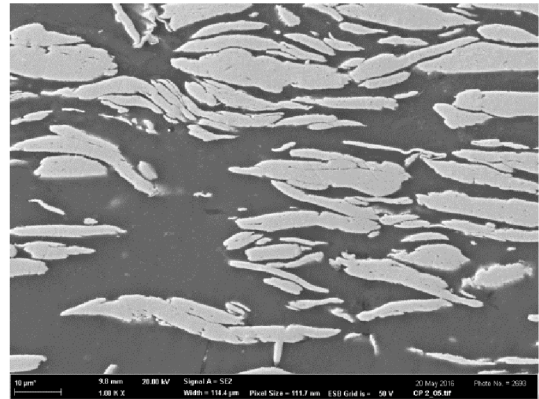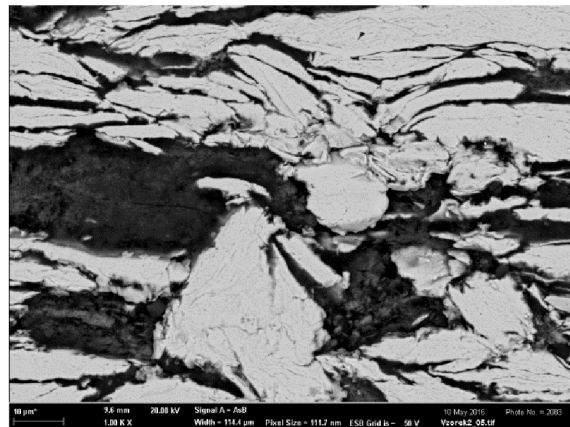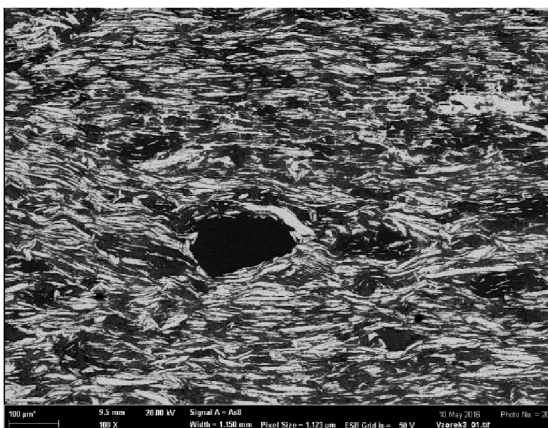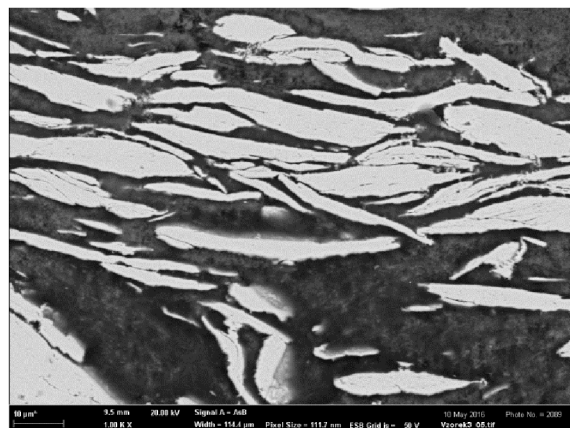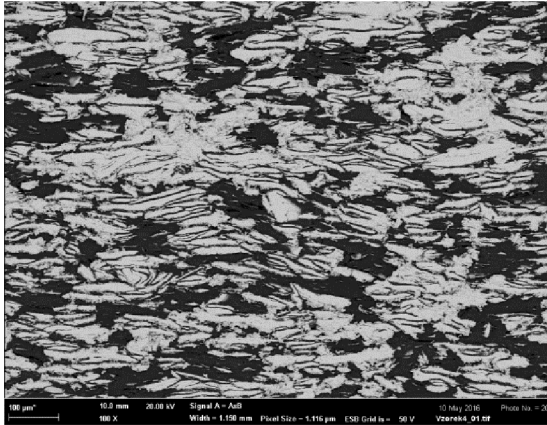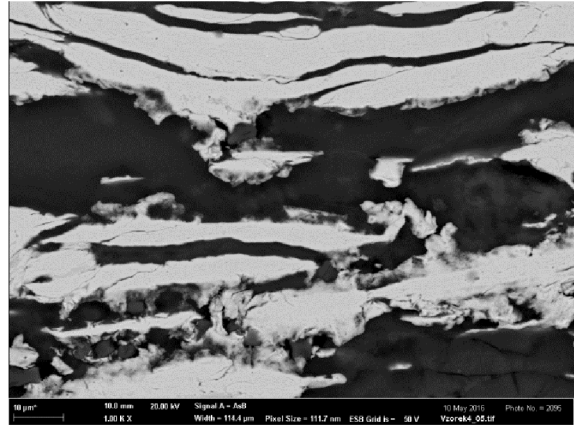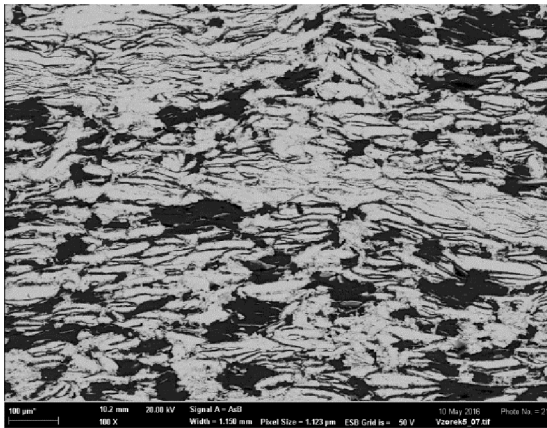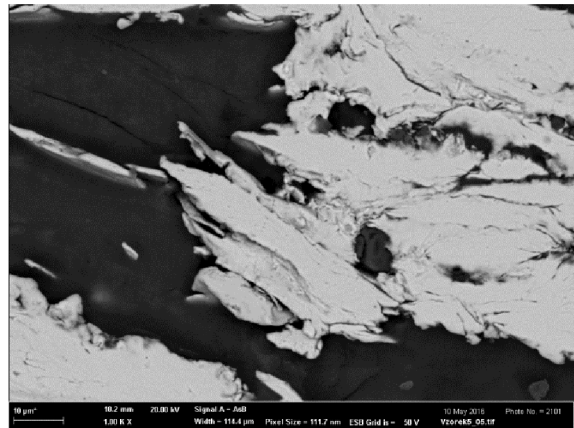

Fig. 4.4 CP1 magnification 1000x
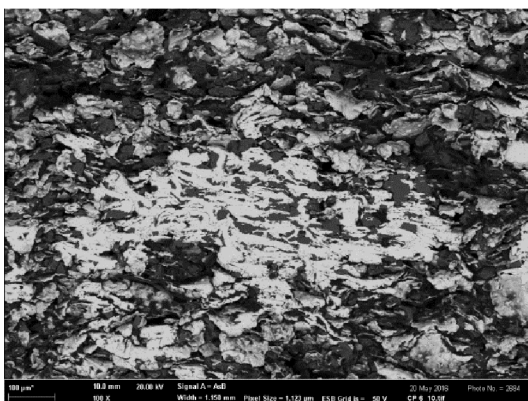
Fig. 4.3 CP2 magnification 100x
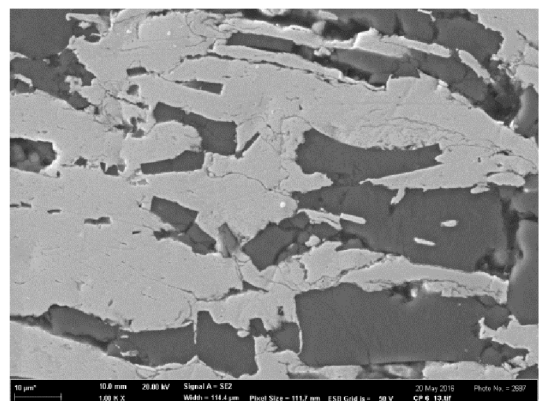
Fig. 4.5 CP2 magnification 1000x

The structure of powder feedstock proved to have and an effect on the structure of compacts too. In case of SPS compaction, Powder 2 seemed to create better bondings and more regular structure than Powder 1. The main difference may be in the

attributes of Al in both powders. As shown in Fig. 3.1 and Fig. 3.2, the Al particles are much bigger in Powder 1, which has a negative effect on Al distribution, shape and sintering possibilities. However, as Fig. 4.2 shows structure of CP1, long sintering time had similar effect on Al as in case of SPS3-2. Although they are very similar, application of pressure during sintering is obvious as the structure of SPS3-2 is much more ordered. Another possible explanation is an effect of much higher pressure applied with CP1 that could help crumble large particles into smaller pieces thus enabling better sintering with Cu. It is then interesting to observe, that same pressure did not have the same effect on CP2 structure, but as already mentioned, specimen CP2 could not be prepared for microscopy analyses as well as the other ones.

Even though Portier et al. claim temperatures between 600-700 °C should produce the best quality compacts, it was not so in this case. [31] However, they used a different approach of preparing the powder feedstock and slightly different composition. After all it seems like the key factor for obtaining a good structure is mainly the temperature, as the finest, most organized and most sintered structures were obtained by sintering at 920 °C, both for SPS and CP specimen.

4.2.3 Chemical and phase composition

Light microscopy, XRD and EDX technologies helped to determine distribution of elements and state of diffusion proces in sitered compacts. Upon examining for all the specimen, 3 structures were distinguished based on their color differences – a „dark" phase, a „yellow phase" and „grey" phase. Based on the knowledge of powder composition it was easy to recognise the „yellow" phase as Cu, the „grey" particles as Ni, but only after examining the specimen by EDX it could be confirmed, that the „dark" phase was Al (Fig. 4.18, Fig. 4.19, Appendix 3). Thus, the heat treatment nor the SPS process influenced in any way the initial structure of amorphous Al. This is also confirmed by the data obtained by XRD (Appendix 2) analyses, which did not recognize any phase structures based on Al.

Fig. 4.18 adequately represents the effect of combination of fine powder feedstock structure and SPS compaction as was observed in all other specimen prepared from Powder 2. When comparing Fig. 4.1 and Fig. 4.18, it is obvious that the boundaries between Cu and Ni are not as sharp and clear after exhibiting the powder to SPS compaction process. Therefore it can be stated that a diffusion process has been executed in some extent, as some remainings of Ni particles are still distinguishable. Only those particles of Ni which were not embedded in Cu matrix as for example shown in Fig. 4.1 did not exhibit almost any degree of diffusion, even if they were close to Cu particles. However, it has to be mentioned that observation of such spots was rather an exception that a rule. This leads to a conclusion that mechanical alloying contributes to better execution of diffusion.

According to the EDX analyses the chemical composition of sintered compacts does not vary from the chemical composition of powder feedstocks (Table 5). All the data obtained have to be considered carefully, because all specimens were analysed in one spot only. Repeated analyses for every specimen would lead to better overall results. The discovered Si particles in SPS1-2 and SPS2-2 specimens have been embedded into the structure most likely during grinding.

However, the XRD analyses revealed interesting phenomenon in SPS compacts. As Table 6 shows, none of the SPS sintered compacts exhibits presence of any other

phase but Cu, even though a proportion of Ni was detected in original powder feedstocks. This may be caused by limited distinctive abilities of XRD device, when all the phases of a proportion smaller than 2% are subjected to measurement error. However on the other hand it confirms the observation made in Fig. 4.18 about well executed diffusion process and creation of solid solution of Cu and Ni. The presence of Ni detected in CP1 and its absence in CP2 also confirms the above mentioned statement about better exhibited diffusion process in case of compacts made out of Powder 2. Presence of Cu-based oxide structures was detected in these specimens, which is a result of exhibiting the specimens to the air when pulled out of tube furnace and water when quenched.

Table 5 Chemical composition of sintered compacts

Specimen	Composition (wt%)				
	Cu	Al	Ni	O	Si
SPS1-1	53	23,6	3,1	20,3	
SPS2-1	63,8	17,6	3,3	15,3	
SPS3-1	48,4	27,3	2,5	21,9	
SPS1-2	50,6	25	4,2	18,8	1,4
SPS2-2	52,7	24,3	3	18,2	1,7
SPS3-2	50,3	27,8	2,6	19,3	
CP1	46,5	34,1	2,9	16,9	
CP2	63,7	23,9	3,8	8,5	

Table 6 Phase composition of sintered compacts

Specimen	Phases and their proportion in specimen
Powder 1	94,6%**Cu**; 5,4%**Ni**
Powder 2	93,2%**Cu**; 6,8%**Ni**
SPS1-1	100% **Cu**
SPS2-1	100% **Cu**
SPS3-1	100% **Cu**
SPS1-2	100% **Cu**
SPS2-2	100% **Cu**
SPS3-2	100% **Cu**
CP1	92% **Cu**; 3,8%**Cu2O**; 2,1%**Ni**; 2,1%**CuO**
CP2	89,9% **Cu**; 9,3%**Cu2O**; 0,8%**CuO**

Fig. 4.6 SPS1-1 magnification 100x

Fig. 4.7 SPS1-1 magnification 1000x

Fig. 4.8 SPS2-1 magnification 100x

Fig. 4.9 SPS2-1 magnification 1000x

Fig. 4.10 SPS3-1 magnification 100x

Fig. 4.11 SPS3-1 magnification 1000x

Fig. 4.12 SPS1-2 magnification 100x

Fig. 4.13 SPS1-2 magnification 1000x

Fig. 2.14 SPS2-2 magnification 100x

Fig. 4.15 SPS2-2 magnification 1000x
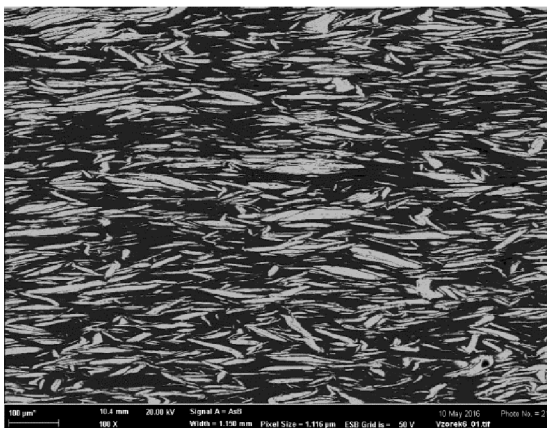
Fig. 4.16 SPS3-2 magnification 100x
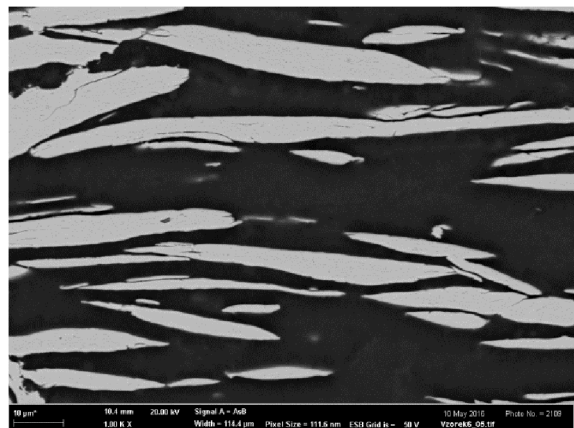
Fig. 4.17 SPS3-2 magnification 1000x
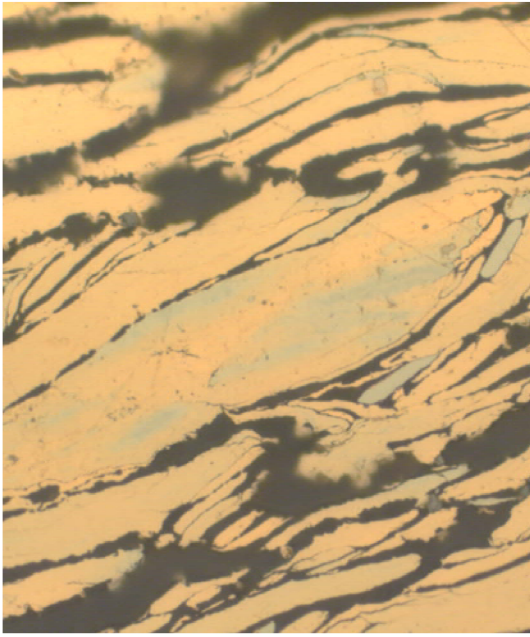
Fig. 4.18 SPS2-2 provided by light microscopy, magnification 100x
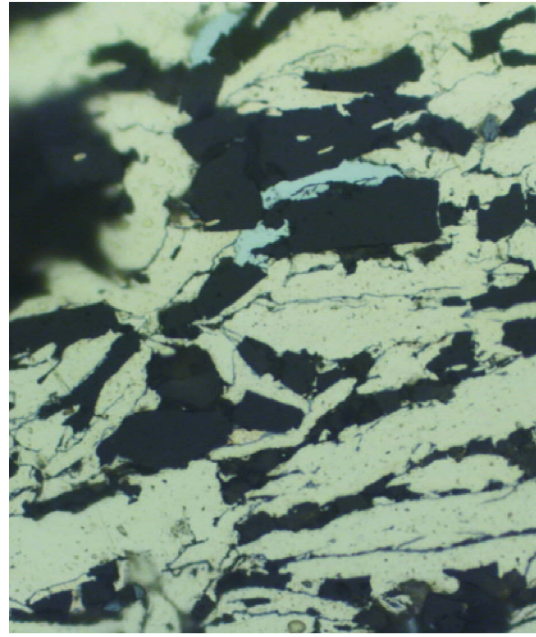
Fig. 4.19 CP2 provided by light microscopy, magnification 100x

5 CONCLUSIONS

In this work the effects of different sintering techniques and parameters were studied, analysed and discussed. Based on the obtained results and observations it can be concluded that:

- MA contributes to better diffusion processes in powder metallurgy compaction and sintering processes, although different milling parameters have to be applied in order to preserve original attributes and of elements and avoid amorphisation
- Best structures were obtained when sintering at the temperature 920 °C for both SPS and heat treatment procedures, temperature 600 °C has showed to be insufficient. Best results were observed in specimen SPS3-2.
- SPS technology combining applied pressure and temperature produces high density compacts with very fine structure and promotes diffusion
- Aluminum did not recover from its initial amorphous state even after being subjected to heat treatment

6 LIST OF IMAGES AND TABLES

6.1 Images

6.2 Tables

7 ABBREVIATIONS AND SYMBOLS

SMA   -   Shape memory alloy
SME -   Shape memory effect
OWSME   -   One-way shape memory effect
TWSME   -   Two-way shape memory effect

8 BIBLIOGRAPHY

[1]   MOHD JANI, J., M. LEARY, A. SUBIC and M.A. GIBSON A review of shape memory alloy research, applications and opportunities. *Materials & Design*. 2014, (56), 1078-1113. DOI: 10.1016/j.matdes.2013.11.084. ISSN 0261-3069.

[2]   CALLISTER, William and David RETHWISCH *Fundamentals of materials science and engineering: SI version*. 4th ed. Hoboken: Wiley, 2013. ISBN 9781118322697.

[3]   SMITH, William and Javad HASHEMI. *Foundations of materials science and engineering*. 5th ed. Boston: McGraw-Hill, 2010. ISBN 9780073529240.

[4]   LIU, Yinong, Yong LIU and J. VAN HUMBEECK Two-way shape memory effect developed by martensite deformation in NiTi. *Acta Materialia*. 1998, **47**(1), 199-209. DOI: 10.1016/S1359-6454(98)00325-5. ISSN 1359-6454.

[5]   STOECKEL, Dieter. The Shape Memory Effect - Phenomenon, Alloys and Applications. In: SCHETKY, L.McD. *Proceedings: Shape memory alloys for power systems*. Palo Alto, CA (United States): Memry Corp., Brookfield, CT (United States), 1995, s. 1-13.

[6]   KAUFFMAN, George and Isaac MAYO. The Story of Nitinol: The Serendipitous Discovery of the Memory Metal and Its Application. *The Chemical Educator* [online]. 1997, **2**(2) [cit. 2016-05-24]. DOI: 10.1333/s00897970111a. ISSN 1430-4171. Available at: http://chemeducator.org/bibs/0002002/00020111.htm

[7]   Technical Characteristics of Flexinol® Actuator Wires F1140Rev I.2. *DYNALLOY, Inc.* [online]. b.r. [cit. 2016-05-24]. Dostupné z: http://www.dynalloy.com/pdfs/TCF1140.pdf

[8]   *Shape Memory Alloy (SMA) Fluid Fitting System: Product Handbook & Engineering Data*. Fullerton, CA, USA, b.r.. Dostupné také z: http://www.aerofit.com/assets/SMABook11-08.pdf

[9]   HARTL, Darren a Dimitris LAGOUDAS Characterization and 3-d Modeling of Ni60ti Sma for Actuation of a Variable Geometry Jet Engine Chevron. In: *SmartLab* [online]. Texas, USA, 2007 [cit. 2016-05-24]. Dostupné z: http://smart.tamu.edu/publications/docs/Proceedings/2007/chchevrons.pdf

[10] MABE, J., F. CALKINS a G. BUTLER Boeing's Variable Geometry Chevron, Morphing Aerostructure for Jet Noise Reduction. In: *47TH AIAA/ASME/ASCE/AHS/ASC STRUCTURES, STRUCTURAL DYNAMICS, AND MATERIALS CONFERENCE* [online]. Reston, Virigina: American Institute of Aeronautics and Astronautics, 2006, s. - [cit. 2016-05-24]. DOI: 10.2514/6.2006-2142. ISBN 9781624100406. Dostupné z: http://arc.aiaa.org/doi/abs/10.2514/6.2006-2142

[11] STOECKEL, Dieter a Thomas VARAN. Use of Ni-Ti shape memory alloys for thermal sensor-actuators. In: EALEY, Mark A. *Active and Adaptive Optical Components*. 1543. San Diego, 1992, s. 382-389. DOI: 10.1117/12.51193. ISBN 9780819406712.

[12] Chevrolet Debuts Lightweight 'Smart Material' on Corvette. In: *General*

Motors [online]. 2013 [cit. 2016-05-25]. Dostupné z: http://media.gm.com/media/us/en/gm/news.detail.html/content/Pages/news/us/en/2013/Feb/0212-corvette.html

[13] *Blockwise Engineering, LLC: Self-Expanding Stent Loaders* [online]. Tempe, AZ, USA, b.r. [cit. 2016-05-25]. Dostupné z: http://www.blockwise.com/blockwise.htm

[14] MIYAZAKI, Shuichi a Kazuhiro OTSUKA. Development of Shape Memory Alloys. *ISIJ International*. 1989, (29), 353-377. ISSN 1347-5460.

[15] BARNES, Clive. Shape Memory and Superelastic Alloys: Copper Applications in Innovative Technology. In: *Innovations* [online]. 1999 [cit. 2016-05-13]. Dostupné z: http://www.copper.org/publications/newsletters/innovations/1999/07/shape.html

[16] HOWELL, P. *On the phases, microconstitutes and microstructures in Nickel-Aluminum bronzes*. The Pennsylvania State University, b.r.. Dostupné také z: http://www.copper.org/publications/pub_list/pdf/A1310-Microstructures-NickelAlumBronzes.pdf

[17] JOHNSON, A. a D. GREY, V. MARTYNOV (ed.), M. BOKAIE (ed.) Superelastic and Shape Memory Single Crystal Cu-Al-Ni: Fabrication and Applications. In: BERG, B., M. R. MITCHELL a J. PROFT *SMST-2006: Proceedings of the 2006 International Conference on Shape Memory and Superelastic Technology*. Pacific Grove, California, USA: ASM International, 2006, 427 - 437 (11). ISBN 978-0-87170-862-5.

[18] PURKHORSHIDI, Sajjad, Mohammad NAEIMI, Nader PARVIN, Seyed ZAMANI a Hamid EBRAHIMNIA. Manufacturing and evaluating Cu-based Shape memory alloy by hot extrusion of PM samples made by Mechanical alloying. In: *Metal 2012: 21st International Conference on Metallurgy and Materials*. Brno, 2012. ISBN 978-80-87294-29-1.

[19] TANG, S.M., C.Y. CHUNG a W.G. LIU Preparation of CuAlNi-based shape memory alloys by mechanical alloying and powder metallurgy method. *Journal of Materials Processing Technology*. 1997, **63**(1-3), 307-312. DOI: 10.1016/S0924-0136(96)02641-6. ISSN 0924-0136.

[20] GILMAN, P.S. a J.S. BENJAMIN Mechanical Alloying. *Annual Review of Materials Science* [online]. 1983, **13**(1), 279-300 [cit. 2016-05-23]. DOI: 10.1146/annurev.ms.13.080183.001431. ISSN 00846600. Dostupné z: http://www.annualreviews.org/doi/abs/10.1146/annurev.ms.13.080183.001431

[21] SURYANARAYANA, C. *Mechanical alloying and milling*. New York: Marcel Dekker, 2004. Materials engineering (Marcel Dekker, Inc.), 22. ISBN 082474103X.

[22] CAO, W. Synthesis of Nanomaterials by High Energy Ball Milling. In: *Understanding Nano* [online]. b.r. [cit. 2016-05-24]. Dostupné z: http://www.understandingnano.com/nanomaterial-synthesis-ball-milling.html

[23] PÉRÉZ-SÁEZ, R., V. RECARTE, M. NÓ, O. RUANO a J. JUAN. Advanced Shape Memory Alloys Processed by Powder Metallurgy. *Advanced Engineering Materials* [online]. 2000, **2**(1-2), 49-53 [cit. 2016-05-25]. ISSN 1438-1656. Dostupné z:

https://www.researchgate.net/profile/Jose_San_Juan2/publication/264268610_Advanced_Shape_Memory_Alloys_Processed_by_Powder_Metallurgy/links/53de9ef00cf2a76fb6680190.pdf

[24] UPADHYAYA, G. *Powder metallurgy technology.* Cambridge: Cambridge International Science Publishing, 2002. ISBN 1 898326 40 1.

[25] JAMES, W. Powder Metallurgy Methods and Applications. In: SAMAL, P. K. a J. W. NEWKIRK *ASM Handbook, Volume 7: Powder Metallurgy.* Materials Park, OH: ASM International, 2015, s. 9-19. ISBN 978-1-62708-087-3.

[26] SURESH, K.R., S. MAHENDRAN, M.S. KRUPASHANKARA a L. AVINASH Influence of Powder Composition & Morphology on Green Density for Powder Metallurgy Processes. *International Journal of Innovative Research in Science, Engineering and Technology* [online]. 2015, **04**(01), 18629-18634 [cit. 2016-05-17]. DOI: 10.15680/IJIRSET.2015.0401037. ISSN 23476710. Dostupné z: http://www.ijirset.com/upload/2015/january/40_Influence.pdf

[27] MARINOV, Valery. *Manufacturing Technology* [online]. 2004 [cit. 2016-05-17].

[28] FERNÁNDEZ, A., J.L. MENÉNDEZ, R. TORRECILLAS a H.U. KESSEL, M. SUÁREZ (ed.) Challenges and Opportunities for Spark Plasma Sintering: A Key Technology for a New Generation of Materials. ERTUğ, Burcu. *Sintering Applications* [online]. b.r. [cit. 2016-05-11]. DOI: 10.5772/53706. ISBN ISBN 978-953-51-0974-7.

[29] AALUND, Robert. Spark Plasma Sintering. In: *Ceramic Industry* [online]. BNP Media, 2008 [cit. 2016-05-16]. Dostupné z: http://www.ceramicindustry.com/articles/88988-spark-plasma-sintering

[30] REGINÁČ, Jan. *TERNARY SHAPE MEMORY ALLOYS POWDER FEEDSTOCK FABRICATION BY ADVANCED MECHANICAL ALLOYING.* Brno, 2016. BACHELOR'S THESIS. VUT. Vedoucí práce Čížek.

[31] PORTIER, Richard A., Patrick OCHIN, Alexandre PASKO, Gennady E. MONASTYRSKY, Andrei V. GILCHUK, Victor I. KOLOMYTSEV a Yuri N. KOVAL Spark plasma sintering of Cu–Al–Ni shape memory alloy. *Journal of Alloys and Compounds* [online]. 2013, **577**, 472-477 [cit. 2016-05-26]. DOI: 10.1016/j.jallcom.2012.02.145. ISSN 09258388. Dostupné z: http://linkinghub.elsevier.com/retrieve/pii/S0925838812004343

9 APPENDICES

Appendix 1: SPS sintering history
Appendix 2: XRD analysis results
Appendix 3: EDX analysis results

SPS1-1

Temperature PV: 174 °C
Temperature SP: 16 °C
Pressure PV: 4.95 MPa
Pressure SP: 5.00 MPa

Position: 49.128   mm
Vacuum: 10.37 V
Thermocouple: 174 °C
Pyrometer: 462 °C

Power Supply DC Volts: -2.49 V
Power Supply DC Current: -993 A

Program # 17   Cu_Al_Ni_600C_8m
Program Status: Reset
Segment: 1/7
Segment Time Remaining: 00:00:00
Program Time Elapsed: 00:00:00

HISTORY

SCREEN
SIZE

PRINT
SCREEN

2016-05-02
11:29:57

DATA LOGGING   On
160502_1_Cu_14Al_4Ni_600C_60MPa_8min_term

2016-05-02   Click: Label for Scale, Chart for Cursor   [Setup]

Temperature PV	Temperature SP	Pressure PV	Pressure SP	Position	Vacuum	DC Current	DC Volts
173.637	16.000	4.955	5.000	49.128	10.376	-993.000	-2.490

52.00

47.00

11:00   11:05   11:10   11:15   11:20   11:25   11:30

[Help]
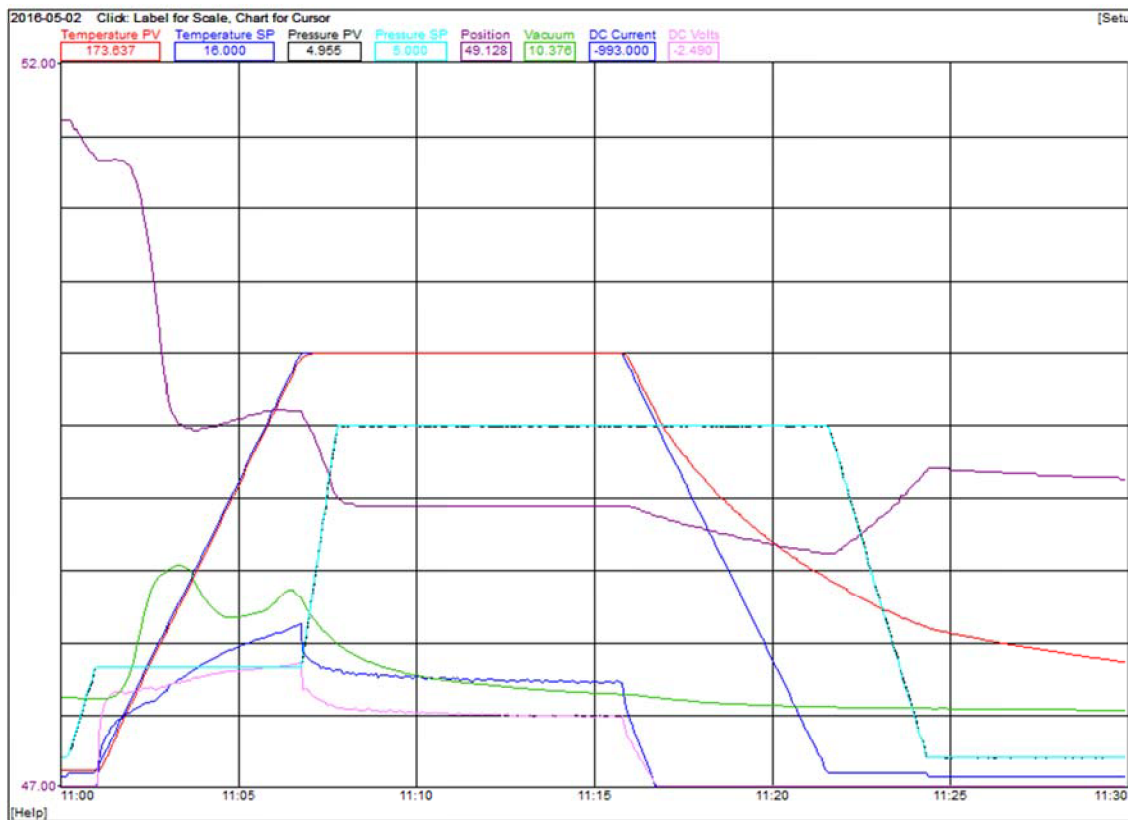
CHART 2   CHART 3   CHART 4

Temperature PV: 125 °C
Temperature SP: 16 °C
Pressure PV: 5.02 MPa
Pressure SP: 5.00 MPa

Position: 49.422 mm
Vacuum: 11.57 V
Thermocouple: 125 °C
Pyrometer: 461 °C

Power Supply DC Volts: -2.49 V
Power Supply DC Current: -993 A

Program # 17   Cu_Al_Ni_600C_8m
Program Status: Reset
Segment: 1/9
Segment Time Remaining: 00:00:00
Program Time Elapsed: 00:00:00

HISTORY

SCREEN
SIZE

PRINT
SCREEN

2016-05-02
16:09:30

DATA LOGGING   On
160502_3_Cu_14Al_4Ni_600C_60MPa_8min_term

SPS2-1

2016-05-02   Click: Label for Scale, Chart for Cursor   [Setup]

Temperature PV	Temperature SP	Pressure PV	Pressure SP	Position	Vacuum	DC Current	DC Volts
125.166	16.000	5.019	5.000	49.422	11.567	-993.000	-2.490

53.00

48.00
14:30   15:00   15:30   16:00   16:30

[Help]

CHART 2   CHART 3   CHART 4
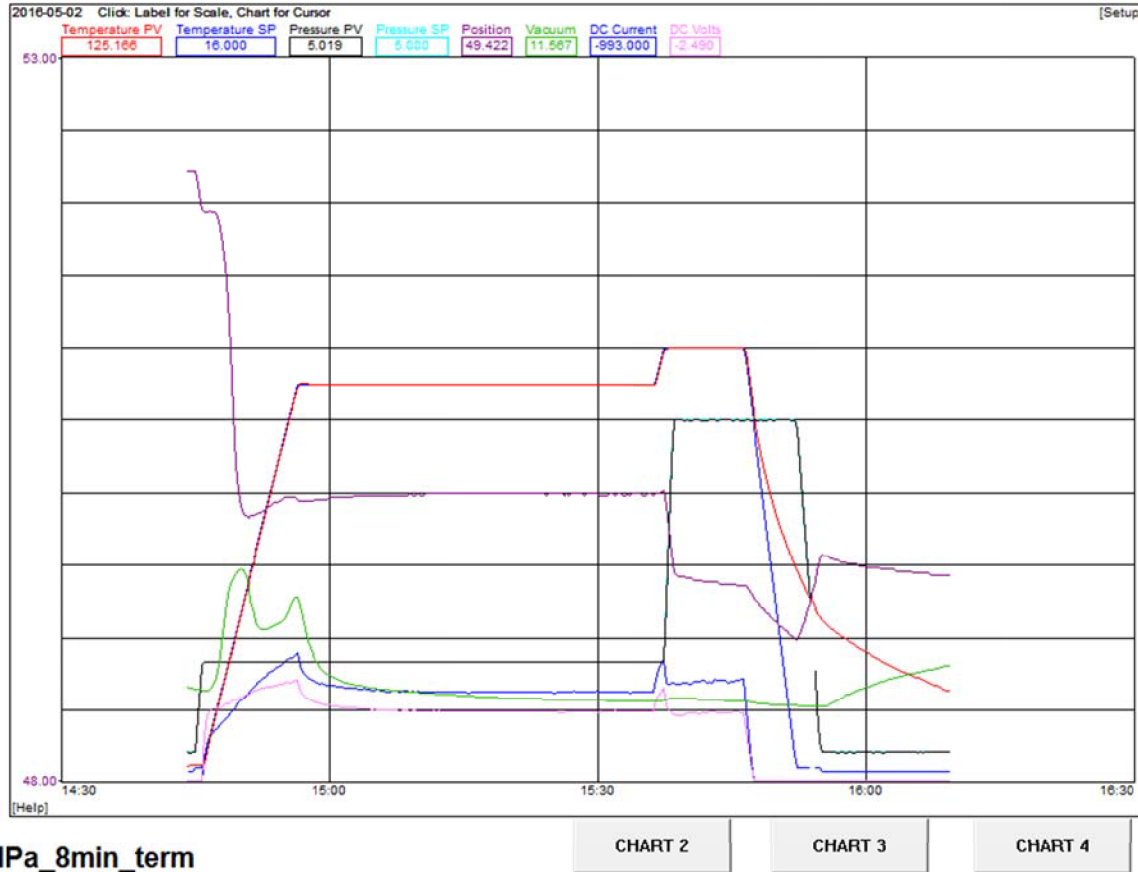
Temperature PV: 115 °C
Temperature SP: 16 °C
Pressure PV: 4.99 MPa
Pressure SP: 5.00 MPa

Position: 48.758 mm
Vacuum: 10.68 V

Thermocouple: 115 °C
Pyrometer: 462 °C

Power Supply DC Volts: -2.49 V
Power Supply DC Current: -993 A

Program # 17   Cu_Al_Ni_920C_8m
Program Status: Reset
Segment: 1/9
Segment Time Remaining: 00:00:00
Program Time Elapsed: 00:00:00

HISTORY

SCREEN
SIZE

PRINT
SCREEN

2016-05-03
11:38:33

DATA LOGGING   On
160503_2_Cu_14AI_4Ni_920C_60MPa_8min_term

2016-05-03   Click: Label for Scale, Chart for Cursor   [Setup]

Temperature PV	Temperature SP	Pressure PV	Pressure SP	Position	Vacuum	DC Current	DC Volts
115.362	16.000	4.955	5.000	48.771	10.669	-993.000	-2.490

[Help]

CHART 2   CHART 3   CHART 4

SPS1-2
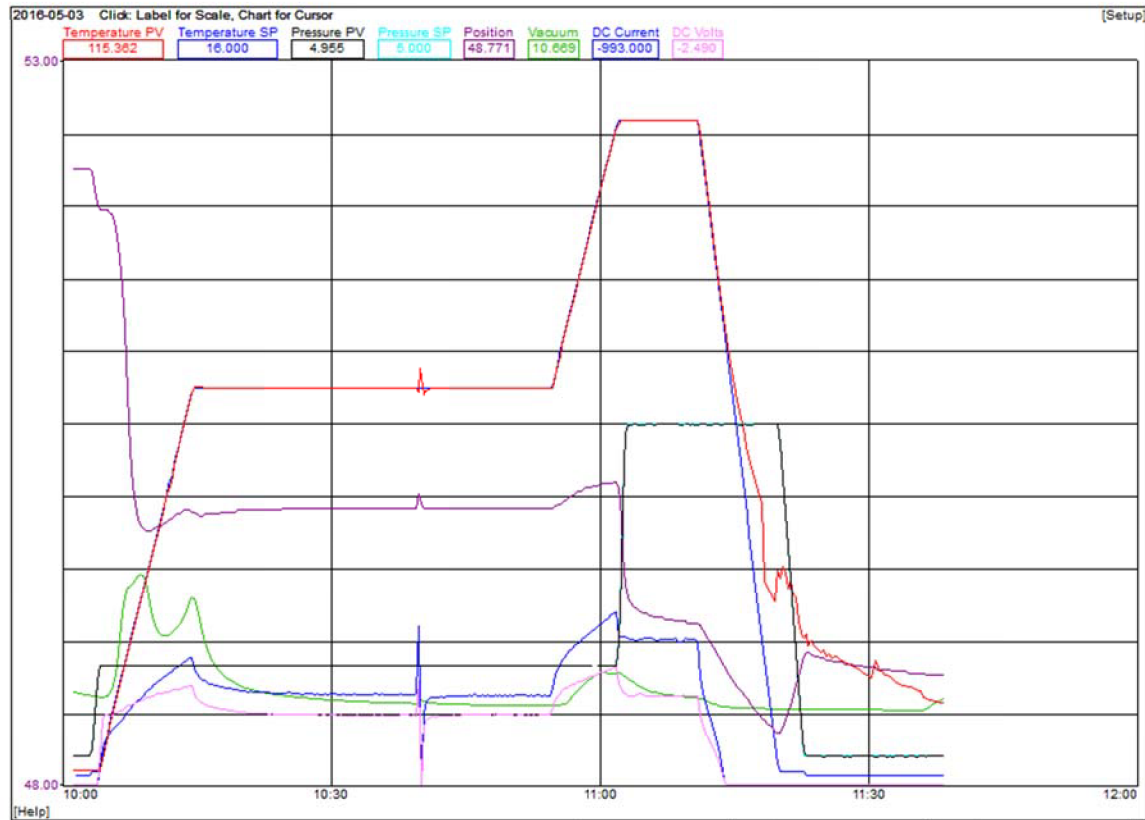
Temperature PV: 180 °C
Temperature SP: 16 °C
Pressure PV: 4.95 MPa
Pressure SP: 5.00 MPa

Position: 48.860 mm
Vacuum: 11.05 V

Thermocouple: 180 °C
Pyrometer: 461 °C

Power Supply DC Volts: -2.49 V
Power Supply DC Current: -993 A

Program # 17   Cu_Al_Ni_600C_8m

Program Status: Reset
Segment: 1/7
Segment Time Remaining: 00:00:00
Program Time Elapsed: 00:00:00

HISTORY

SCREEN SIZE

PRINT SCREEN

2016-05-02
13:39:58

DATA LOGGING   On
160502_2_Cu_14Al_4Ni_600C_60MPa_8min_term

2016-05-02   Click: Label for Scale, Chart for Cursor   [Setup]

Temperature PV	Temperature SP	Pressure PV	Pressure SP	Position	Vacuum	DC Current	DC Volts
180.272	16.000	4.987	5.000	48.860	11.047	-993.000	-2.490

[Help]

CHART 2   CHART 3   CHART 4
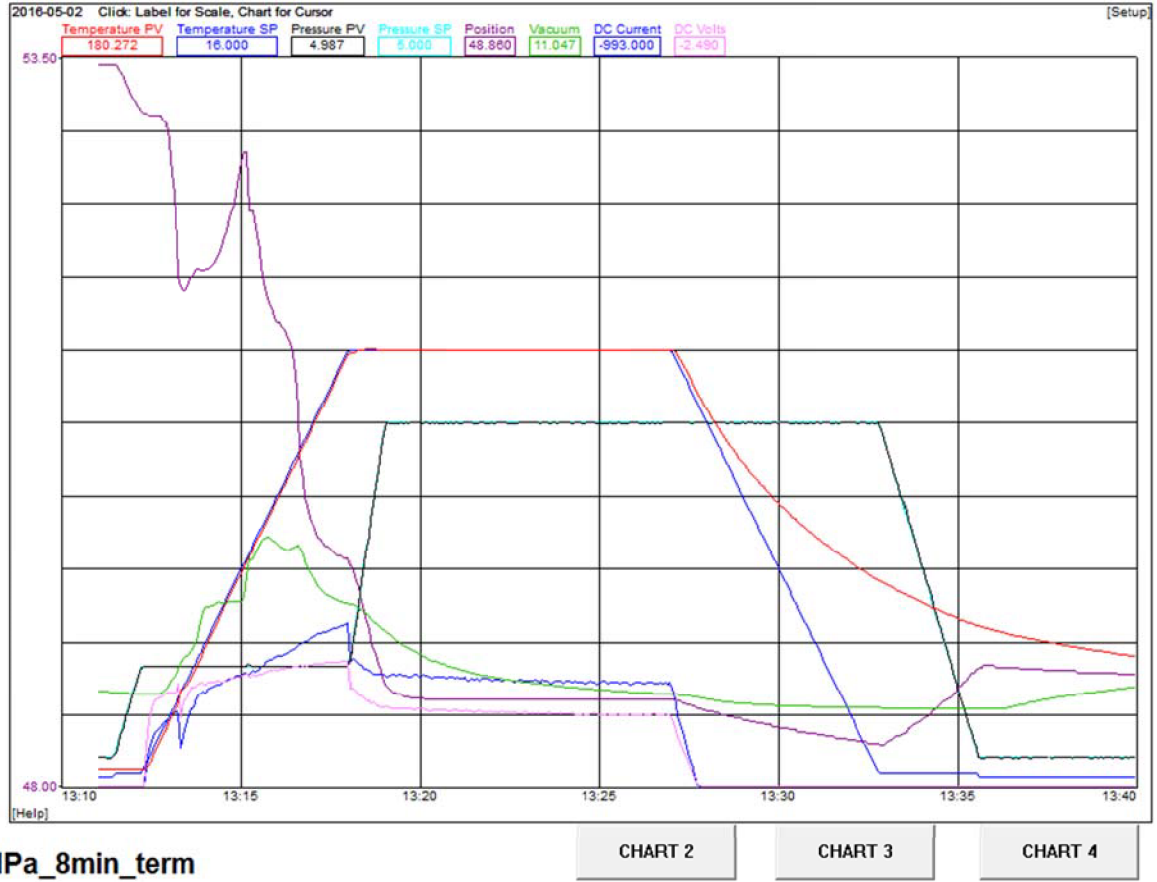
Temperature PV: 108 °C
Temperature SP: 16 °C
Pressure PV: 4.99 MPa
Pressure SP: 5.00 MPa

Position: 48.873 mm
Vacuum: 10.35 V

Thermocouple: 108 °C
Pyrometer: 462 °C

Power Supply DC Volts: -2.49 V
Power Supply DC Current: -993 A

Program # 17   Cu_Al_Ni_600C_8m
Program Status: Reset
Segment: 1/9
Segment Time Remaining: 00:00:00
Program Time Elapsed: 00:00:00

HISTORY

SCREEN SIZE

PRINT SCREEN

2016-05-03
09:17:42

DATA LOGGING   On
160503_1_Cu_14Al_4Ni_600C_60MPa_8min_term

2016-05-03   Click: Label for Scale, Chart for Cursor   [Setup]

Temperature PV	Temperature SP	Pressure PV	Pressure SP	Position	Vacuum	DC Current	DC Volts
108.635	16.000	5.019	5.000	48.873	10.349	-993.000	-2.490

53.50

48.00 07:30   08:00   08:30   09:00   09:30

[Help]
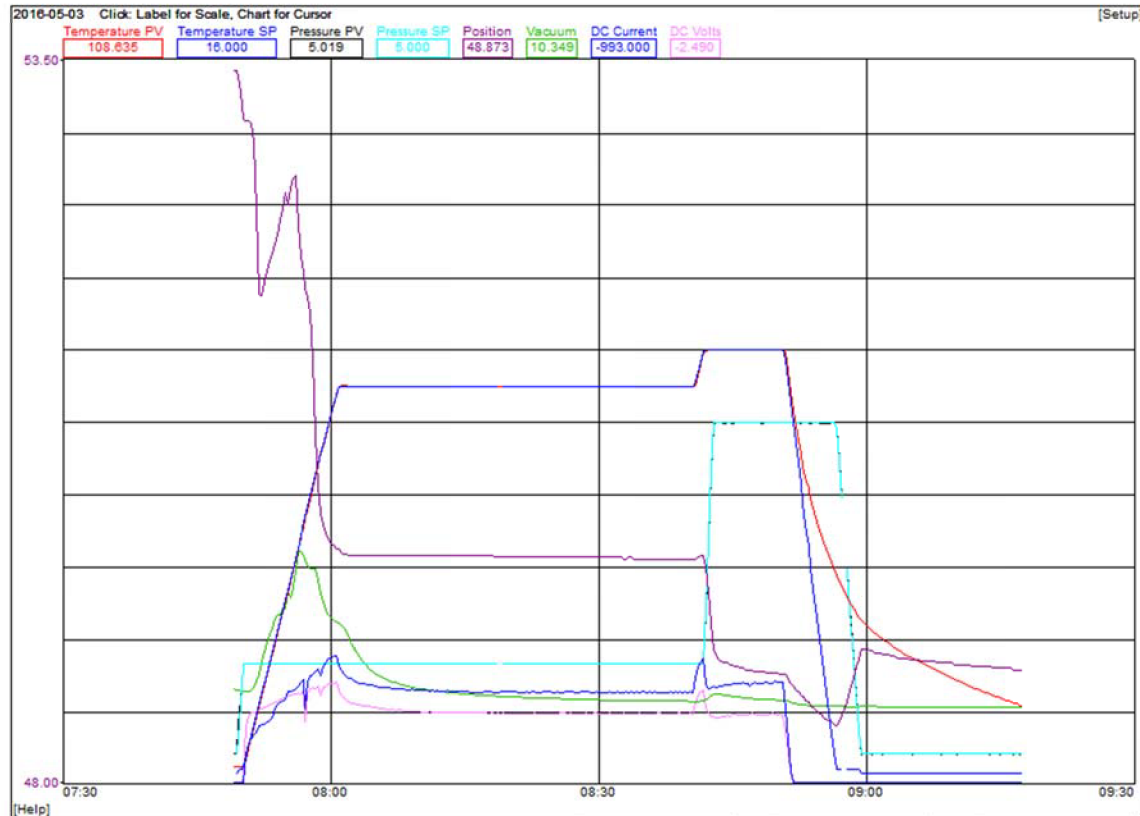
CHART 2   CHART 3   CHART 4

SPS2-2

page 47

SPS3-2

Temperature PV: 105 °C
Temperature SP: 16 °C
Pressure PV: 4.99 MPa
Pressure SP: 5.00 MPa

Position: 48.362 mm
Vacuum: 10.93 V
Thermocouple: 105 °C
Pyrometer: 462 °C

Power Supply DC Volts: -2.49 V
Power Supply DC Current: -993 A

Program # 17 Cu_Al_Ni_920C_8m
Program Status: Reset
Segment: 1/9
Segment Time Remaining: 00:00:00
Program Time Elapsed: 00:00:00

HISTORY

SCREEN
SIZE

PRINT
SCREEN

2016-05-03
14:59:00

DATA LOGGING On
160503_3_Cu_14Al_4Ni_920C_60MPa_8min_term

2016-05-03   Click: Label for Scale, Chart for Cursor   [Setup]

Temperature PV	Temperature SP	Pressure PV	Pressure SP	Position	Vacuum	DC Current	DC Volts
105.025	16.000	4.987	5.000	48.362	10.928	-993.000	-2.490

53.50

48.00

13:00   13:30   14:00   14:30   15:00

[Help]

CHART 2   CHART 3   CHART 4
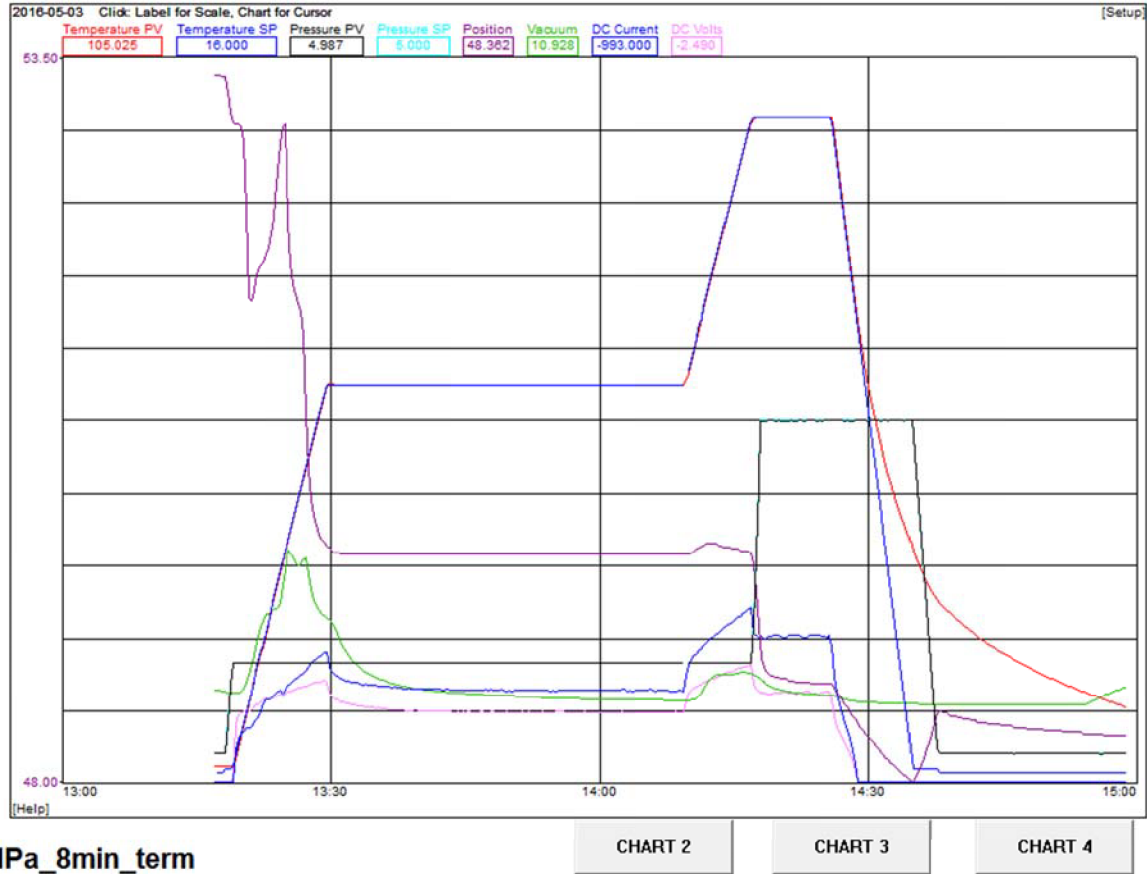
Appendix 2: XRD analysis results

Powder 1 and compacts thereof
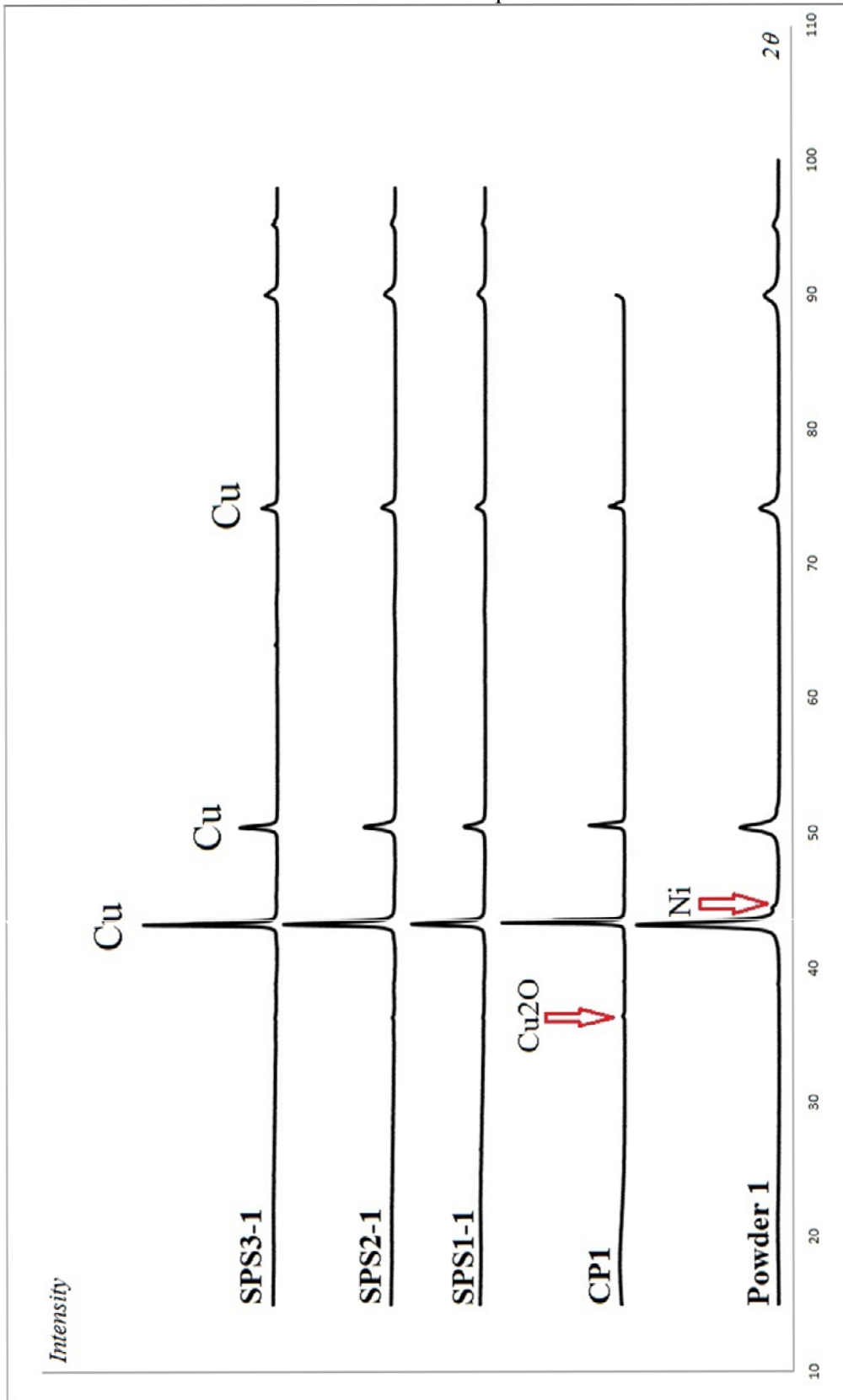
Powder 2 and compacts thereof

EDX analysis results

EDS Layered Image 1

Map Data 1

O Ni Cu Al Electron

1mm

Cu Kα1

500µm

Al Kα1

500µm

Ni Kα1

500µm

O Kα1
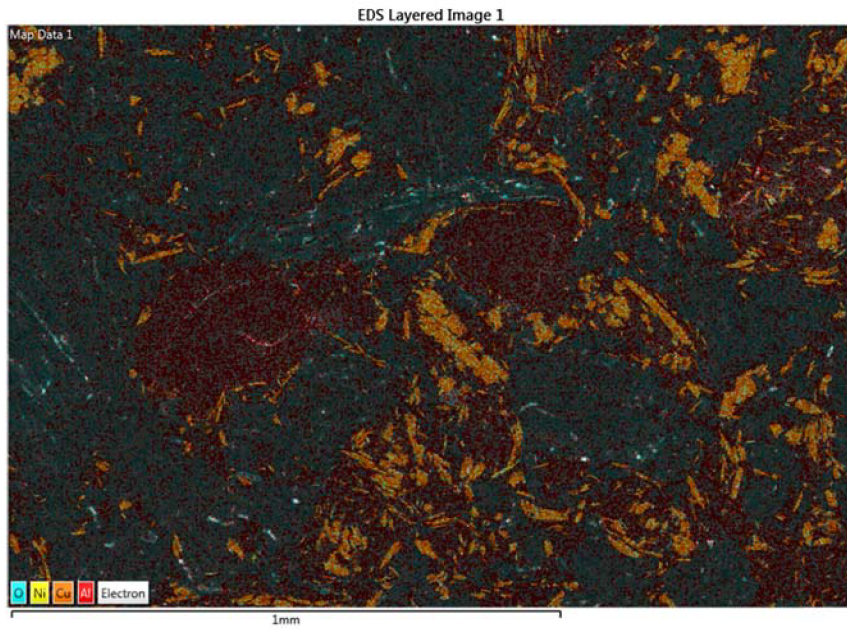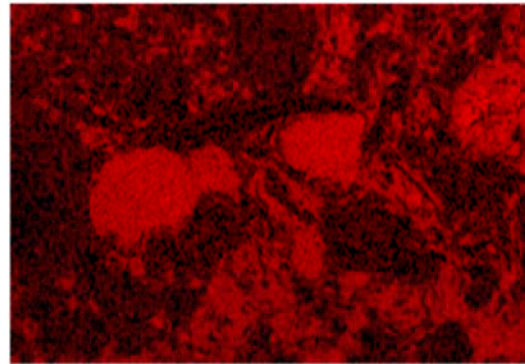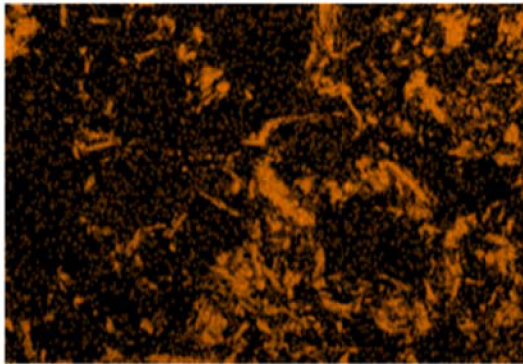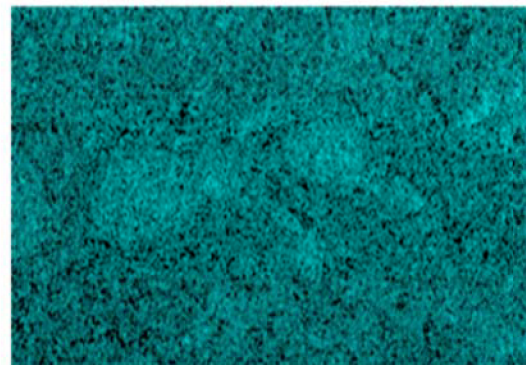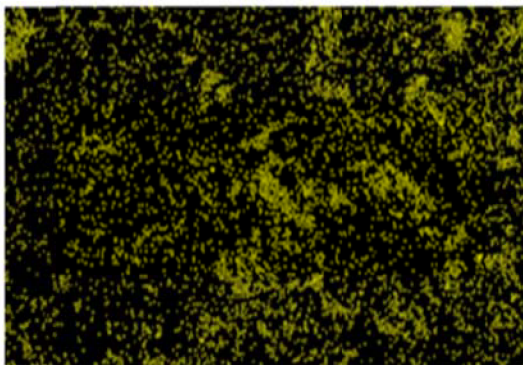
500µm

Powder 2

EDS Layered Image 1

Ni Al Cu O Electron

500µm
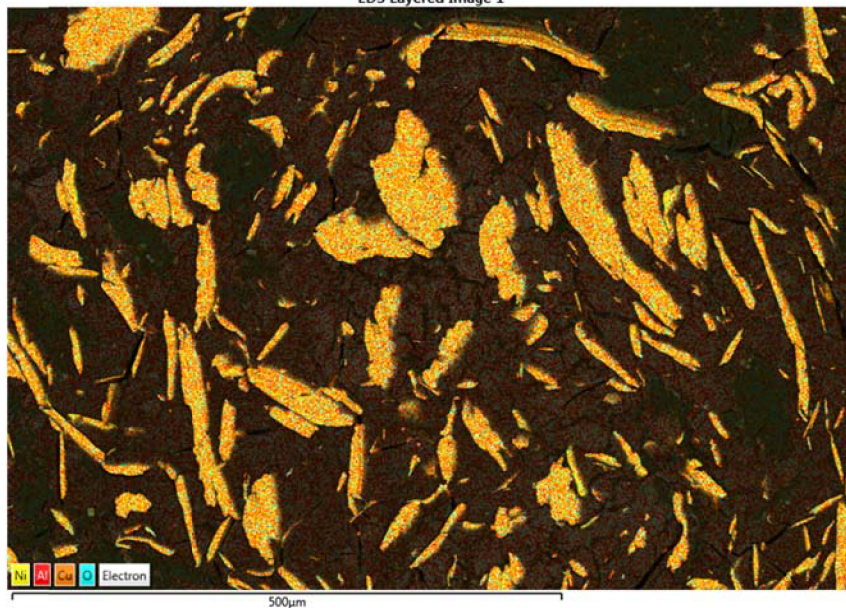
Cu K series
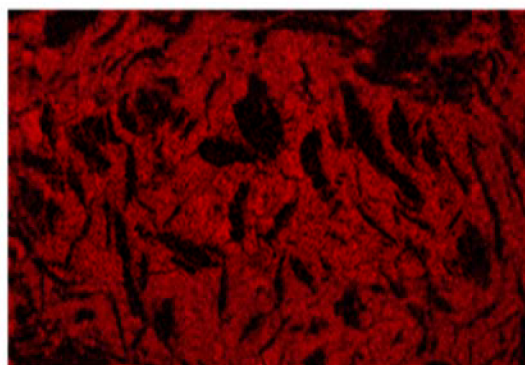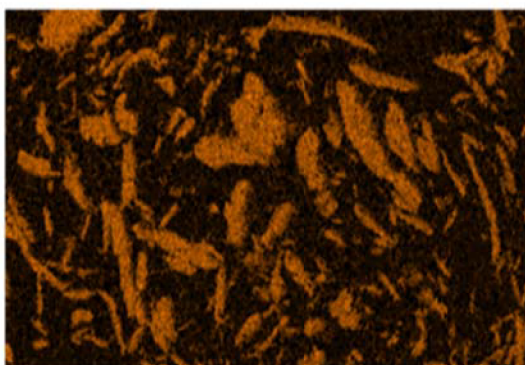
250µm

Al K series

250µm

Ni K series
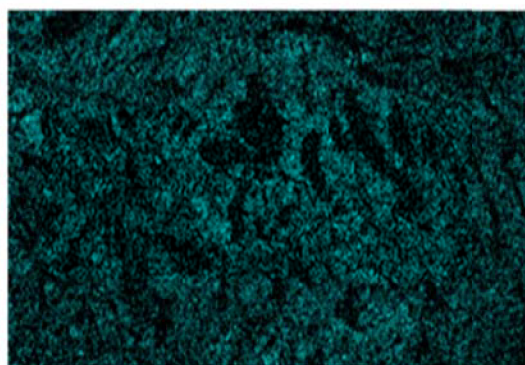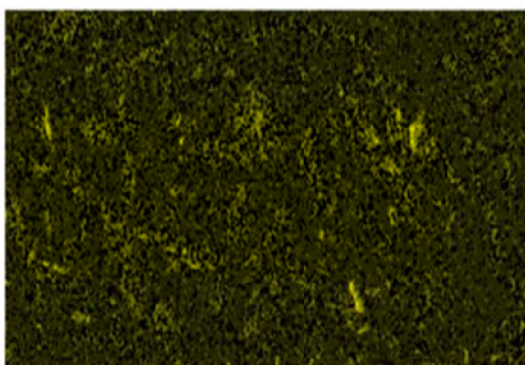
250µm

O K series

250µm

CP1

EDS Layered Image 2
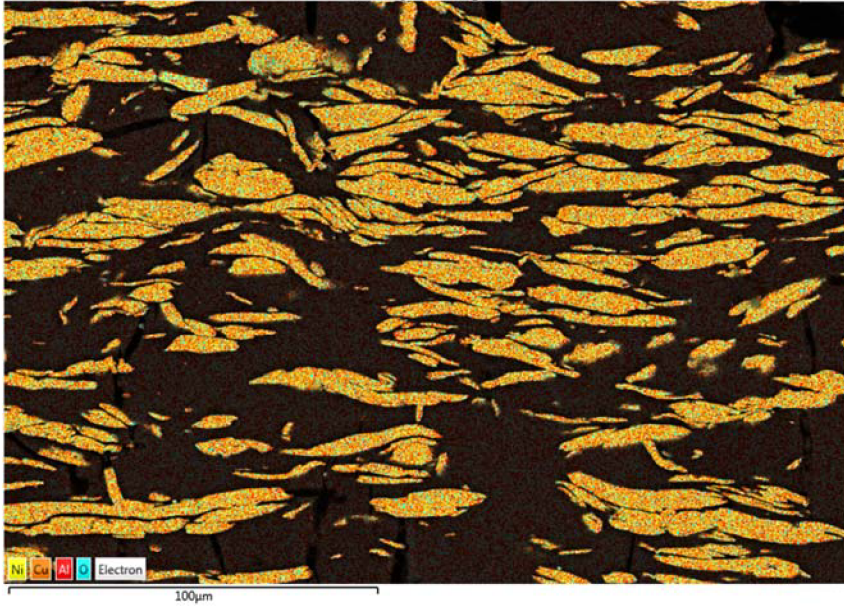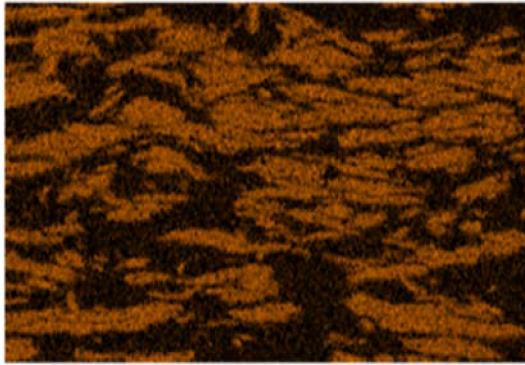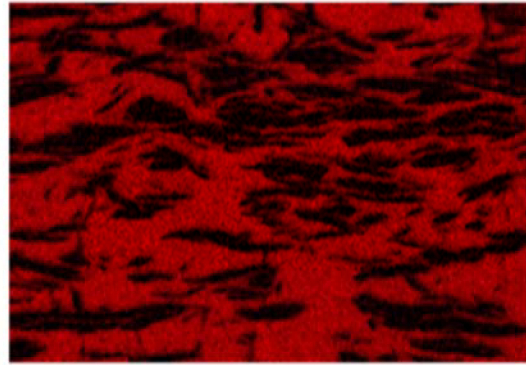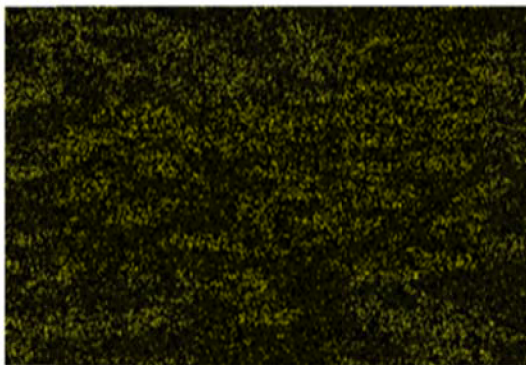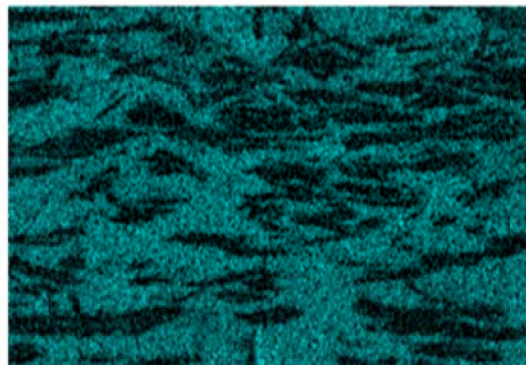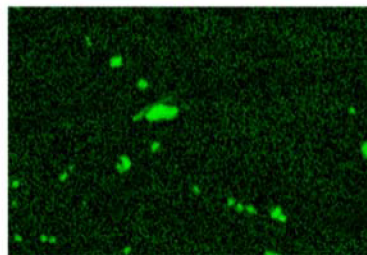

Cu K series

50μm

Al K series

50μm

Ni K series

50μm

O K series

50μm

CP2
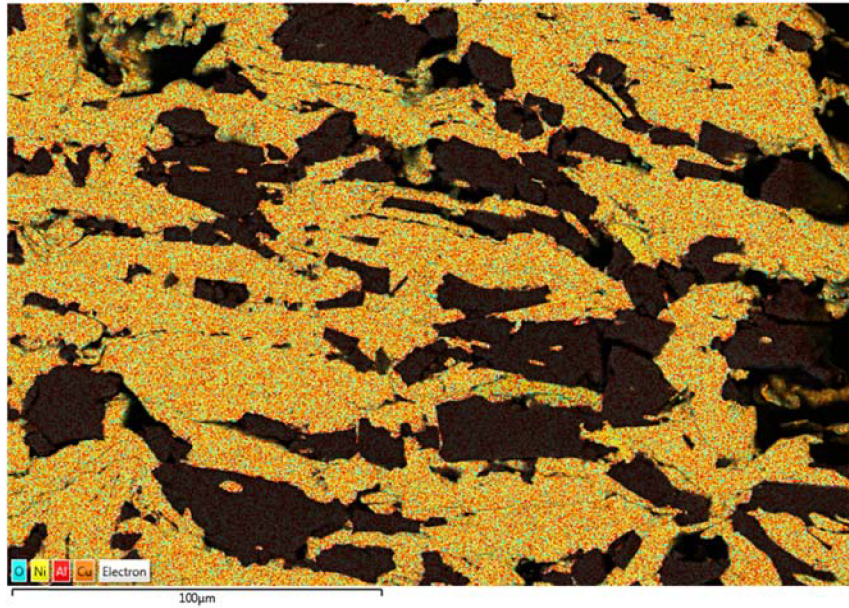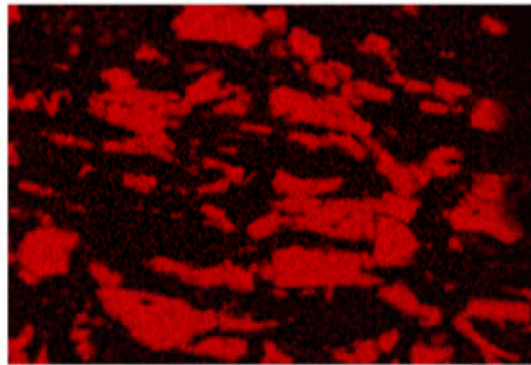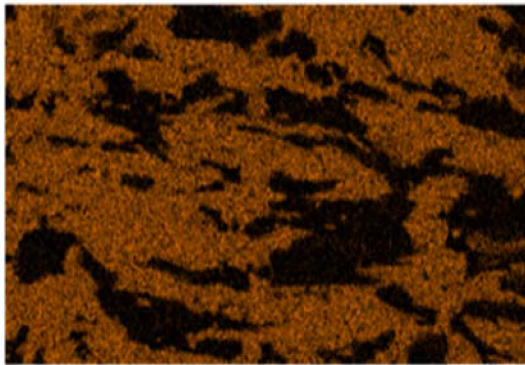
Cu K series

Al K series
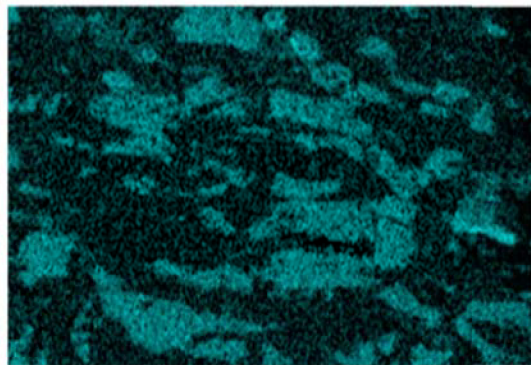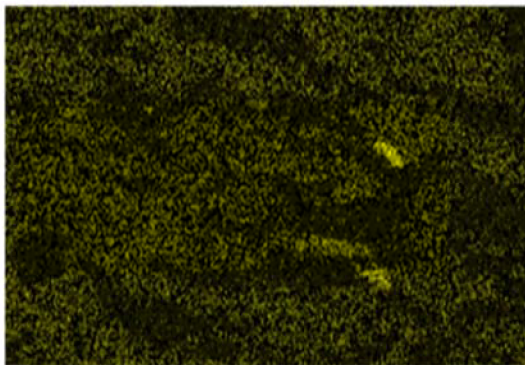
Ni K series

O K series

SPS1-1

EDS Layered Image 1

100μm

Cu K series
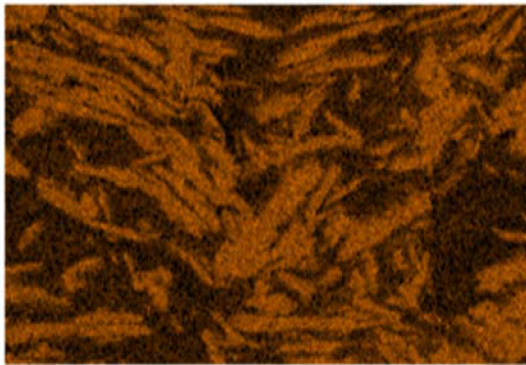
50μm

Al K series

50μm

Ni K series
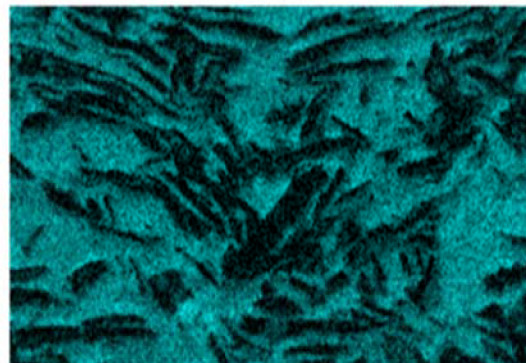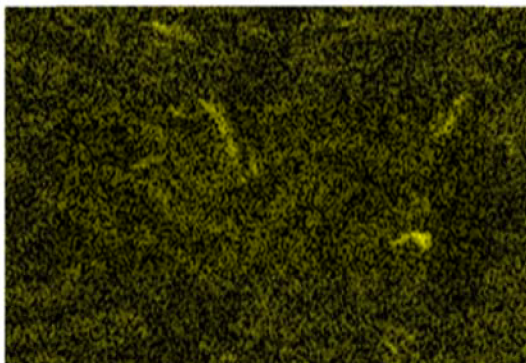
50μm

O K series

50μm

SPS2-1

EDS Layered Image 2
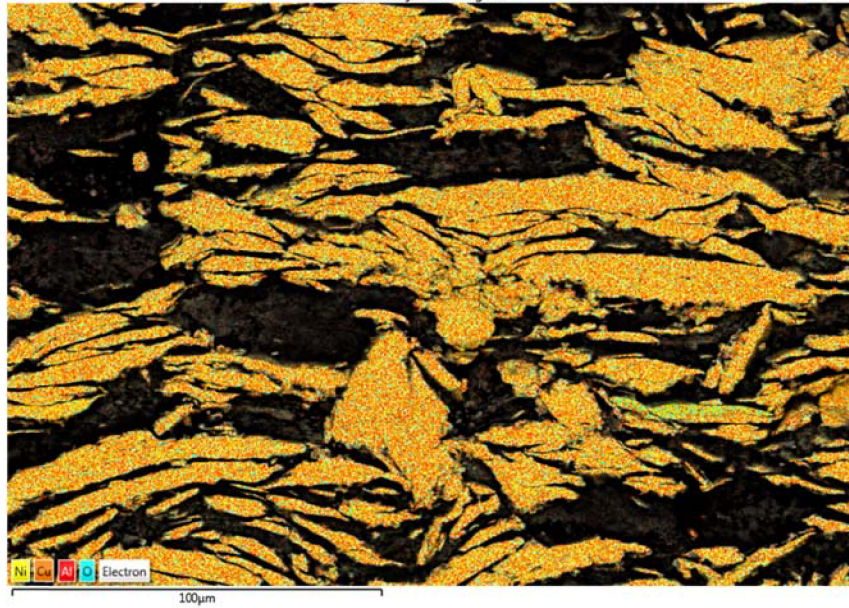
Cu K series

Al K series
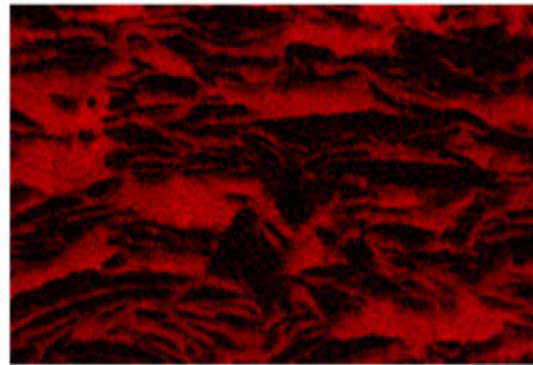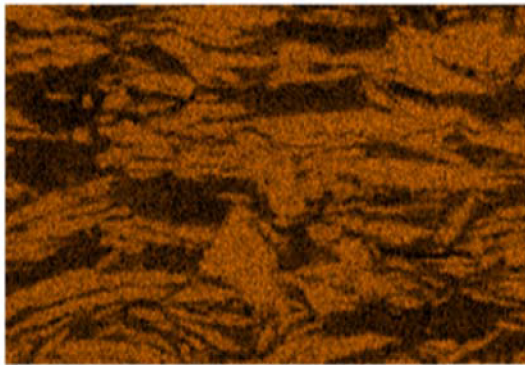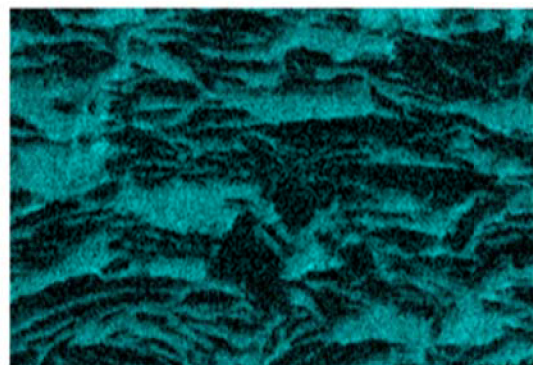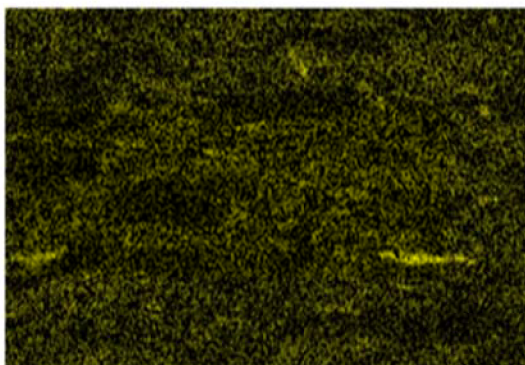
Ni K series

O K series

SPS3-1
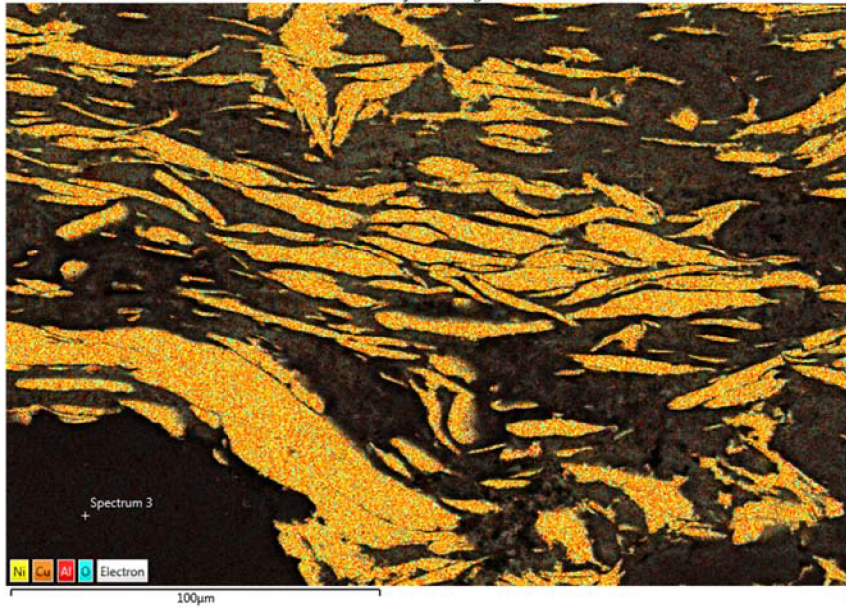
Cu K series
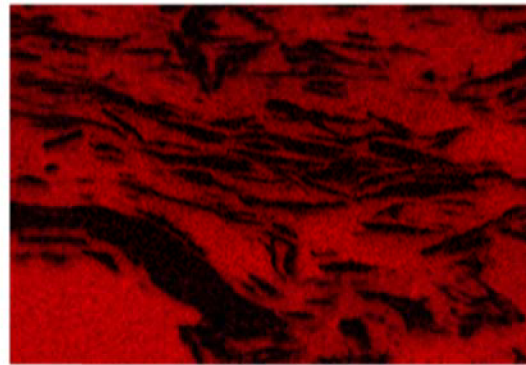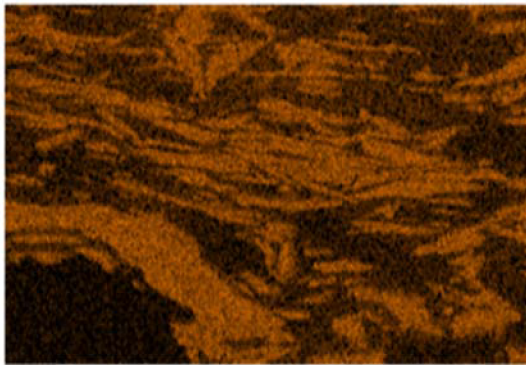
Al K series

Ni K series
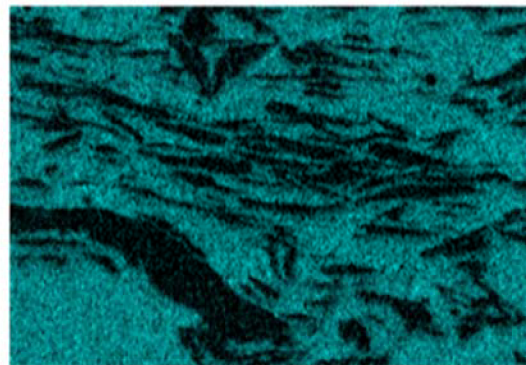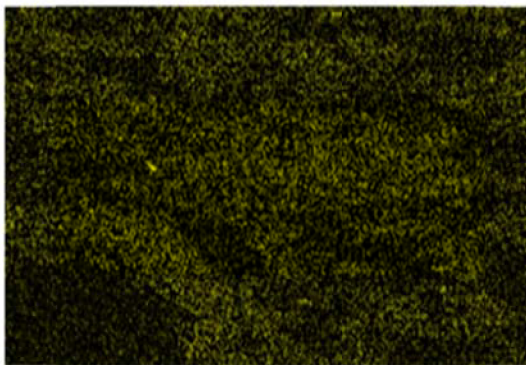
O K series

SPS1-2

EDS Layered Image 4
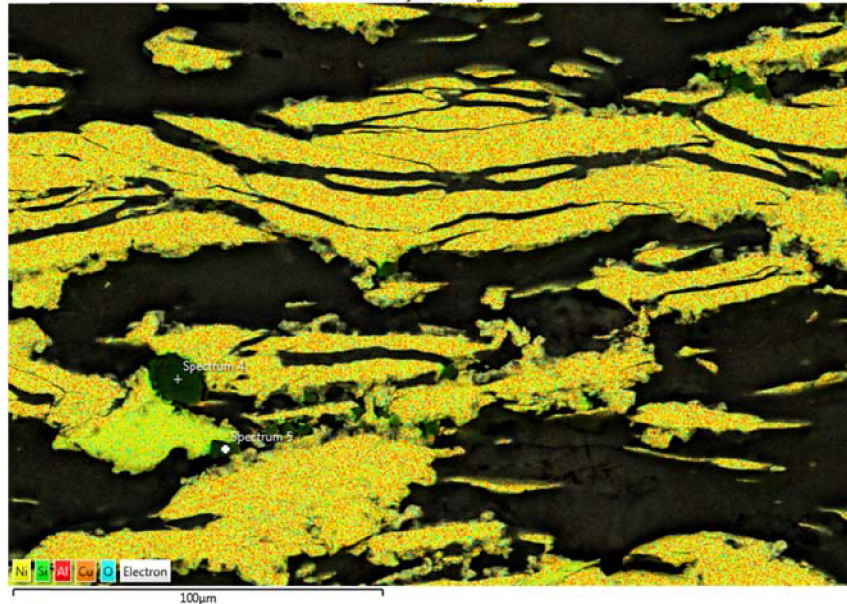
Cu K series
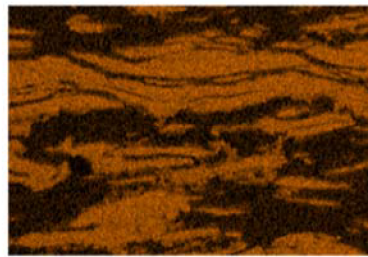
Al K series
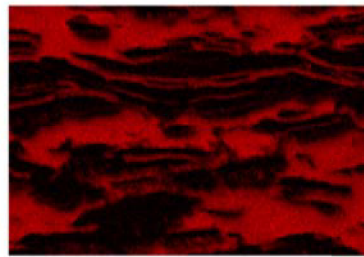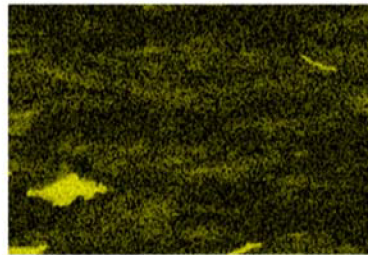
Ni K series
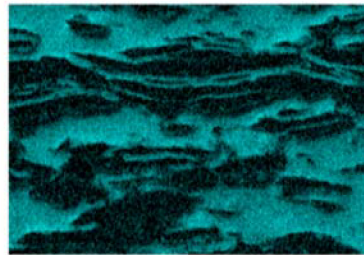
O K series
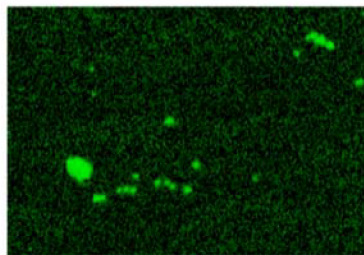
Si K series

SPS 2-2

EDS Layered Image 5
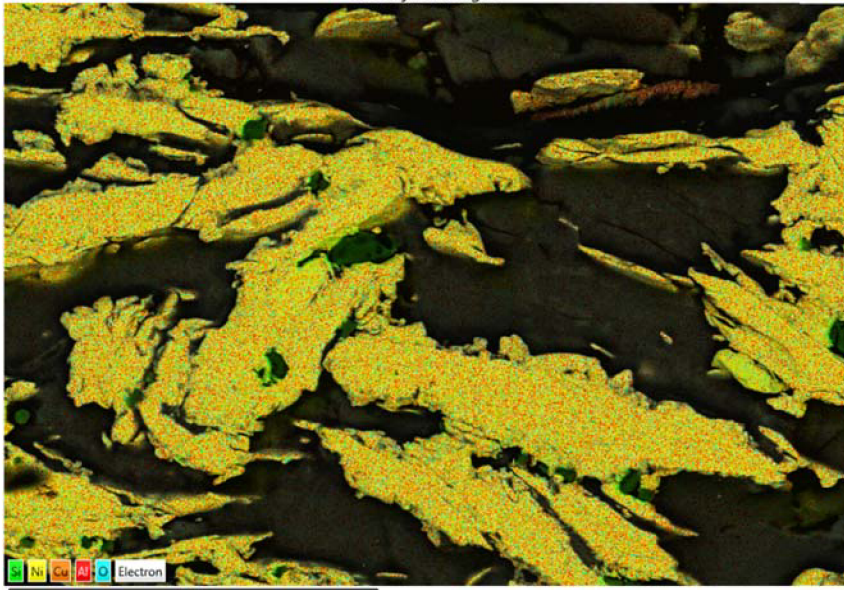
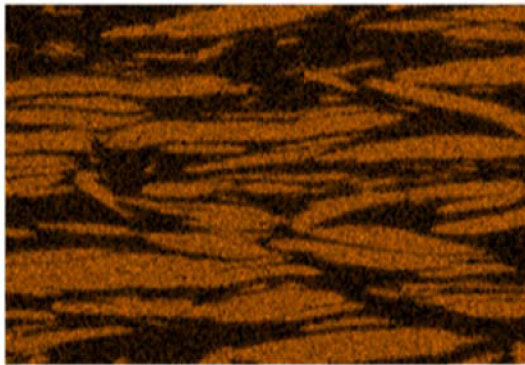Cu K series

Al K series
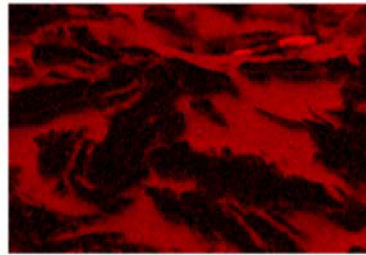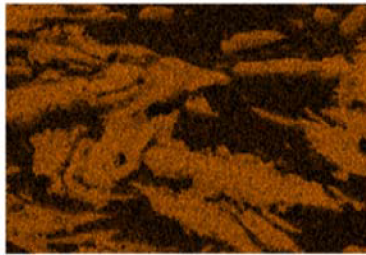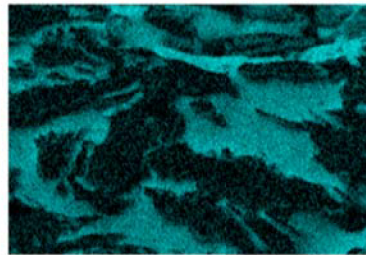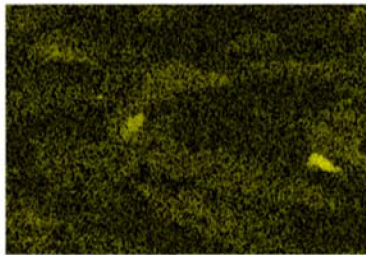
Ni K series

O K series

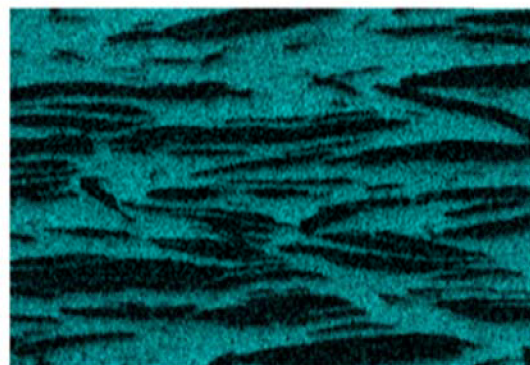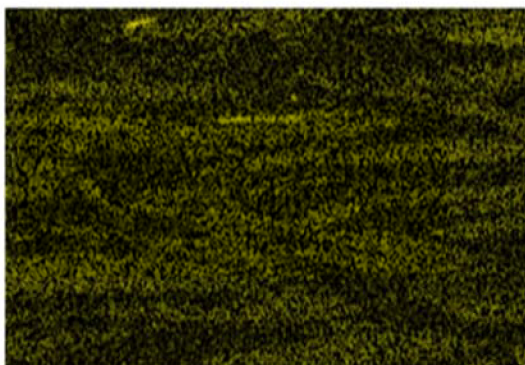Si K series

SPS3-2

EDS Layered Image 6

Cu K series

Al K series

Ni K series

O K series